Printability and Environmental Testing using Silver-based Conductive Flexographic Ink Printed on a Polyamide Substrate

Kathryn O. Cole
Rochester Institute of Technology, School of Print Media
69 Lomb Memorial Drive, Rochester, NY 14623 (USA)
E-mail: katieocole@yahoo.com

Abstract
The effect of simulated environmental exposure conditions (high heat, freezing temperature, rain, and vacuum pressure) on the performance of a silver-based conductive flexo ink printed on a polyamide (nylon 6,6) substrate was examined. Conductivity, density, color, adhesion, abrasion resistance and creasing were evaluated.

The tested environmental variables did not have an effect on the performance quality of silver conductive flexographic ink when printed on a polyamide substrate for the 85 – 100% solid ink density levels. Rain and temperature had the greatest impact on print performance in the 70–80% tint range. Exposure to these elements affected adhesion properties of the ink to the substrate, which lead to a negative effect on the conductivity and abrasion performance.

This study indicated an antenna printed at common ink density levels using a silver-based flexographic printing ink on a polymeric film is a possible solution for the implementation of printed RFID components. This is a manufacturing option that can bring the packaging industry from a "slap and stick" RFID labeling method to an actual inline production method that can be applicable to both primary and secondary package tagging needs. Lastly, the study utilizes common ink testing procedures that will be useful in the development of standards for the production of printed RFID components in packaging applications.

Introduction
An area of growth opportunity for the print industry driven by demand from large retail and manufacturing customers is printed electronics[1]. One of the current main products of the printed electronics industry is printed radio frequency identification (RFID) components. RFID technology has been in use for several years but advances in printing materials and methods have finally permitted the possibility of a fully printed RFID tag. This advancement has lead to a potential market share in the billions of dollars. Harrop[1] believes that by the year 2016, the RFID market will grow to a value of $26.23 billion. Printers can capitalize on this market by creating a low cost but highly effective fully printed RFID tag for use in product packaging. To achieve this, significant research in the area of materials and end-use performance testing is needed to develop a set of standards for the industry to follow.

The research conveyed in this study provides valuable information for materials testing of a commonly used silver-based flexographic ink for use in typical product packaging applications. The researcher exposed sample prints to varying simulated environmental conditions a package might endure. A set of ink-testing procedures was conducted to determine the effect, if any, on the performance of the ink by comparison to a controlled environmental condition.

Research Questions

1.) Can conductive ink withstand conditions a printed RFID tag would be exposed to in the primary or secondary level packaging supply chain?

2.) Does exposure to environmental elements have an effect on the performance of a silver-based conductive flexographic ink?

3.) What is the optimum ink density level for printing RFID components with a silver-based conductive ink?

Theoretical Basis

Determination of Ink Testing

End uses of various packaging applications were considered in the selection of ink testing procedures for this experiment. Storage and shipping environments were the main consideration for the choice of simulated environments, however, primary packaging applications were also considered. Ink tests of conductivity, density, color, adhesion, abrasion resistance and creasing were the chosen ink testing methods. This was based on standard end use ink testing procedures set forth by the examination of a study published by Jonathan Collins of Precisia, formerly a subdivision of Flint Ink, in RFID Journal[2].

The study by Collins indicates that one of the critical factors to the successful printing of conductive antennas is thickness of the ink film or level of ink density. At the time, there was not a set standard in place with regards to minimum required density level to achieve an acceptable level of conductivity of an ink patch for the use of antenna production[2]. Therefore, it was determined that conducting the chosen tests over several ink density levels would give valuable data with regards to this matter. This is why a proofing plate with varying tint percentages from 100 – 60% density levels was chosen.

The key ink quality factors that Collins suggests should be considered as standard testing procedures for printed antenna production are color, optical density, rub resistance, the effect of creasing and the adhesive qualities of the ink. He also goes on to say that these qualities should be tested with mind to electrical resistivity, crease resistance, temperature, and humidity effects on the performance of the inks[2]. These were key factors that drove the setup of the thesis testing procedures and selection of simulated environmental conditions.

Nylon Substrates

Nylon along with most linear polymers is a glass at low temperatures. As the temperature is increased, the polymer changes from a glass to a rubber at a certain point. This is known as the glass transition temperature or Tg. Nylon being a crystalline polymer, remains thermoplastic or flexible above the Tg level until it reaches the crystalline melting temperature (Tm), in which it begins to melt and transform into a liquid state. For nylon 6,6 these two states occur at Tg= 113° F (45° C) and Tm= 512.6° F (267° C)[3].

Nylon 6,6 film is a viscoelastic material. This means that it has the characteristics of both solid and liquid states[3]. Nylon 6,6 film possess the characteristics of the glassy or brittle state at room

temperature (70° F, 21.1° C), the state in which the print samples for this study were created and also at 45° F (7.2° C), the temperature at which the rain condition was simulated. It also exhibits characteristics of the rubbery state at the temperature of 140° F (60° C), which is the temperature that the heat condition was simulated.

Color Space

The form of color space system that was used in this study is the CIE LAB (L*a*b*) system. CIE stands for Commission Internationale de l'Eclairage or International Commission on Illumination. This system uses a measuring instrument (in the case of this study, an X-Rite DTP 22 Model handheld spectrophotometer) to sample a color and produce a numerical representation of that color. The use of the CIE LAB color system allows the quantification of the color to be device independent through the incorporation of special calculations that allows the mimicking of human vision[4]. In this experiment a determination of 2° observer angle with a D50 Illuminant at a 45° angle was measured to mimic the human eye's vision at a close up distance. The CIE LAB system identifies a specific color by coordinating 3 different measurements (L*a*b*) to a position in a 3D color space. The L* stands for lightness, a* represents the position of the color on a red-green axis, and b* represents the position of the color on a yellow-blue axis[4].

Rheology

Rheology is the study of deformation and flow. Viscosity is the property of fluids that indicates resistance to flow. When a force is applied to a volume of material a displacement (deformation) occurs. In relation to printing inks, the concentration of dissolved or dispersed pigments in the ink can sometimes cause more resistance to flow. An increase in viscosity is known as shear thickening[5]. Shear thickening is a common occurrence with conductive inks because the metallic particles that created conductivity in the ink are often larger than traditional pigments. Therefore, there are often shear thickening problems with conductive inks and the press setting must be adjusted accordingly.

Surface Tension

Surface tension, in terms of the printing industry, is defined as the property of a substrate that relates to how receptive the surface of the substrate is to accepting printing inks[6]. In ink, the molecules at the surface are held together more strongly to those directly associated with the surface. This occurrence forms a surface "film" which has a force greater than the force acting upon the molecules below the surface of the liquid. Surface tension is typically measured in dynes/cm, the force in dynes required to break a film of length one centimeter. Water at 68^{o} F (20° C) has a surface tension of 72.8 dynes/cm. The surface tension of the ink and the substrate were measured to ensure that the ink had sufficient wetting (ability of the ink to adhere to the surface of the substrate when printing at a certain speed) capabilities to create an acceptable print sample. In order for this to be true, the ink had to possess a lower surface tension than that of the substrate. For proper adhesion to occur, the dyne level of the ink should be ten dynes/cm lower than the dyne level of the substrate[7]. If the ink did not have a lower measurement, the ink would not "stick" to the surface of the substrate. Subsequently, the substrate would need to be corona treated to raise the surface tension thus allowing the ink to transfer to the substrate[8]. The surface tension of the nylon 6,6 film used in this experiment measured 50 dynes/cm and the ink used measured 40 dynes/cm. Therefore, it was determined that the ink did possess sufficient wetting capabilities and the substrate did not need corona treatment.

Primary Packaging
Primary packaging is defined as packaging that immediately envelopes a product. It provides most of the strength and the moisture, vapor or grease barrier needed to safeguard a product's purity, potency and integrity from the time it leaves the assembly line until it's used by the consumer. Examples of primary packaging include blister packs, clamshells and trays[9].

Secondary Packaging
Secondary packaging is defined as material used primarily to give additional physical protection to the outside of a primary package. Examples of secondary packaging include cartons, containers, pallets, cardboard boxes, padded bags, and polythene wrap[10].

Role of Nylon in Packaging
Because nylon has many desirable properties such as good thermal, chemical and oil/grease resistance and also good formation properties it is a material that works well as solution for various primary and secondary packaging[11]. Many packaging uses of nylon film are for food and pharmaceutical "clean packaging" needs[12]. It is also used in blister pack applications where it is vacuum or thermo formed[13].

Definition of Ohms/square
Ohms/square is a quantitative method to measure surface resistivity of a material. Gene Chase of ETS, Inc.[14] defines surface resistivity as the resistance between two opposite sides of a square and is independent of the size of the square or its dimensional units. This term is used to describe any dimension of a resistive material and is especially useful in describing thin and thick film antennas because of their variance in size and amount of conductive material used in the manufacture of these devices. The basic principle of using ohms/square when referring to surface resistivity is to divide the surface of the conductive plane (in the scope of this experiment, the surface of the antenna) into any number of squares (in this case centimeters) and measure resistivity in ohms over the distance of the predetermined square. This will indicate the level of resistance to conductivity of the material being measured. The lower the resistance measurement in ohms/square, the more conductive the material is[14].

Determination of Acceptable Resistance Limitation
In the production of RFID antennas, there is not a set standard level of maximum permitted resistance of a conductive material. This is because the conductivity level that is needed to create a functional antenna is dependent upon the read range needed for the tag and also the level of data capabilities of the tag. Antennas that require a longer read range require a higher conductivity level and thus demand a lower acceptance limitation level for surface resistivity. For the scope of this project it was determined that an acceptable limit of resistivity is 25 ohms/square or less. This was derived from the examination of US patent number 6,870,516[15]. In this patent, Aisenbrey establishes that a desirable usable range of resistivity for the production of RFID antennas using a conductive loaded resin-based material is between 5 and 25 ohms/square[15].

Methodology

Substrate

The substrate that was used in this experiment is a polyamide (PA) commonly known as nylon. Nylon is classified as a condensation copolymer. It is a linear thermoplastic polyamide that contains the amide group as a recurring part of its chemical chain. Nylon can be made through the condensation of amino acids that contain both amine and acid functional groups in a single molecule, or they can result from the condensation of diamines and dibasic acids This material is created through the condensation polymerization of hexamethylene diamine and adipic acid[13].

In this experiment, DuPont DARTEK® cast nylon 6,6 film was used to create the print samples. This film was chosen because it is a common film used in the production of bags, tubing, sheets, and sleeves for packaging purposes. It is usually used in film form as a single component or combined into multilayer structures with other polymers in a film. Some of the properties of this film are that it retains its properties over a broad temperature range as it remains flexible as low as -100°F (-73°C) and it will withstand temperatures up to 450°F (232°C). Dependent on environmental conditions, it has good barrier resistance to gases, odors, oils, and greases but is hydrophilic, so it tends to retain moisture. It has an O2 permeability of 3-5 cc/100in^2/day It has a thickness of 0.60 mil to 5.0 mil[16]. For this experiment the substrate was cut into five by nine inch sheets.

To ensure material specifications prior to the samples' print run for the testing process, the researcher conducted a test using a Fourier Transform Infrared (FTIR) spectrometer. Infrared (IR) spectroscopy is a chemical analytical technique that detects the vibration characteristics of chemical functional groups in a sample (in this case, DuPont DARTEK®). When infrared light interacts with the sample's matter, the chemical bonds present in the sample will contract and stretch. When this happens, certain chemical functional groups will absorb the IR radiation in a specific wavenumber. These specific wavenumbers are identifiable in a graph of the spectrum that can be created with the aid of a computer program that interprets the IR data. The chemical functional groups are seen in the peaks and valleys of the spectrum graph[17]. The FTIR spectrum of the substrate sample confirmed the material is nylon 6,6.

The final step in preparing the substrate for printing was to determine the surface tension of the substrate and compare it with the surface tension of the ink. This was done to ensure there would be effective adhesion of the ink to the substrate and to determine that corona treatment of the film was not needed. Surface tension is the work per unit area required to reshape a liquid. It is measured in dynes/cm. For the ink to wet the surface of a substrate, the surface tension of the ink must be lower than the substrate surface tension[18]. A dyne test was performed to ensure that the substrate that was going to be used in this experiment possessed a surface tension higher than the ink. This was done using a set of dyne solutions that ranged from 30 to 60 dynes/cm. In the performance of this test on the DuPont DARTEK® film, it was determined that the dyne level of the substrate was 50 dynes/cm. This number was then compared to the surface tension of the ink and determined that corona treatment of the substrate was not needed because the surface tension of the substrate was higher than that of the ink.

Ink

The ink that was used for this experiment was silver RFID antenna flexographic ink. This water-based silver conductive ink is formulated for use in flexographic printing methods and cures through evaporation of solvents over a period of time. The exact ink formulation is not known, but it is primarily composed of a suspension of finely milled silver (Ag) particles in a resin, solvent, and additives solution. Some of the known properties of the ink are that it is approximately 900cps pre-shear viscosity and is 90% solids[19].

It is important to note that a property of this type of ink is reactivity. Because the metallic particles are reactive, the vehicles they are suspended in must be inert to prevent a potentially hazardous reaction. Another important property of conductive metallic inks are that they attempt to provide a printed surface that can mimic a true metal surface. To do so, the pigments are specially treated and size graded to help determine their orientation in the print ink film. This ensures that the metal flakes are flat and stack on top of each other to promote conductivity; however, this tends to cause problems with cohesion. Metallic inks also have a high specific gravity and are prone to settling. This is especially possible in a low viscosity, water-based ink used in flexographic printing[6].

To ensure that this ink would adhere to the surface of the substrate used in this experiment, the surface tension of the ink was measured using the Fisher Scientific Surface Tensiomat® 21. The surface tension of the ink was measured at 40 dynes/cm. Therefore, it was determined that the ink did possess sufficient wetting capabilities.

Printing

Print samples were made using a K Motorized Printing Proofer manufactured by RK Print Coat Instruments. A patterned anilox (Double 8 Wedge Plate – Model EP 5102/2 Rev.K) was used to create the print sample. The anilox plate used had 150 lines/inch (60 lines/cm) with varying tint patches that had 100-95-90-85-80-75-70-60% density values[20].

To determine the optimal printing conditions required to replicate printing on press, the researcher made several prints adjusting the impression, stereo, and doctor blade pressure until an even ink-film thickness—the amount of ink transferred to the printing substrate, usually measured in microns—and acceptable visual appearance was achieved. This was determined by creating a *kiss* impression where the least amount of pressure needed to create a consistent image was reached. The researcher evaluated the image at kiss impression to make sure that the image had solid lines with no excess ink deposit. Adjusting the rollers provided more or less ink flow onto the substrate, which caused the ink film thickness as well as the appearance of the print to change. The image that was created from this process was used as a visual reference for comparison when print samples for use in the experiment were created (Figure 1).

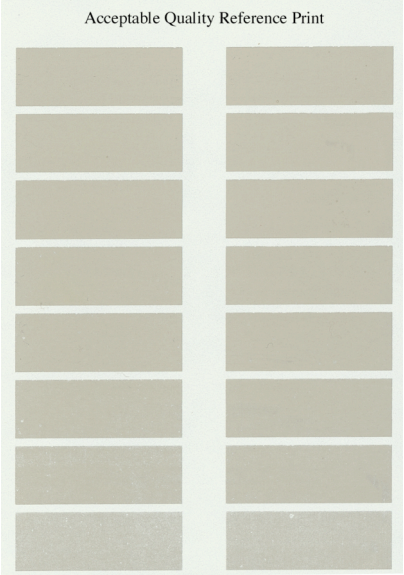

Figure 1. Acceptable quality reference print

The optimal settings used in creating this print were recorded and duplicated to create the print samples for the experiment. These settings include 2.65 for the right and 2.70 for the left of the impression roller, 2.95 for the right and 3.45 for the left of the stereo roller, and 5.70 for the right and 6.36 for the left of the doctor blade. The optimal press speed was determined to be a setting of 4. This process was considered to be the calibration of the proofer.

Print Samples

The print sample was printed five times using the flexographic proofer on the nylon substrate. Five sets of these prints were created for use in the five different inks tests and were exposed to the four environmental conditions, and five prints were created for use as a control set. A set of print samples consists of five prints for the control condition and five prints that will be exposed to an environmental condition. There are 10 prints per set, and there were a total of five sets of print samples created for the four different environmental conditions for a total of 40 prints.

	Heat Set	Control Set #1	Freeze Set	Control Set #2	Vacuum Set	Control Set #3	Rain Set	Control Set #4
Conductivity Test A	Print 1	Print 1	Print 1	Print 1	Print 1	Print 1	Print 1	Print 1
Density/Color Test B	Print 2	Print 2	Print 2	Print 2	Print 2	Print 2	Print 2	Print 2
Adhesion Test C	Print 3	Print 3	Print 3	Print 3	Print 3	Print 3	Print 3	Print 3
Abrasion Test D	Print 4	Print 4	Print 4	Print 4	Print 4	Print 4	Print 4	Print 4
Creasing Test E	Print 5	Print 5	Print 5	Print 5	Print 5	Print 5	Print 5	Print 5

Table 1. Print sample labels used

*All prints were allowed a drying period of 24 hours and reacclimation period of one hour before being subjected to environmental conditions and ink testing procedures.

Environmental Exposure

The simulation of typical environmental packaging conditions was performed by creating a set of four 24-hour periods of exposure to a certain condition and one controlled condition.

Control Set

Control sets of prints (five samples) were created for comparison to each of the four environmental condition samples. The samples were printed according to the optimal print settings that were specified in the calibration of the proofer. Each control set was printed concurrently with the environmental set for which it was compared to and was allowed the same curing period (24 hours) as the set of prints for environmental exposure. Also, since each of the environmental exposure samples required an additional 1-hour acclimation period after removal from the environmental condition before conducting testing procedures, this was also allowed for the control samples. The same ink testing procedures performed on the environmental exposure sets were performed on the control set. The notation that was used to identify the control set of prints in the data recording process was CS#1, CS#2, CS#3, and CS#4, each corresponding to one of the four environmental conditions.

Environmental Conditions

Heat Condition (HC). The purpose of creating a heat exposure condition was to subject the print samples to the environment that a package would endure in its lifecycle, whether through environments it would be exposed to in shipping as a secondary packaging application or environments it would be exposed to as a primary packaging application, The heat exposure was accomplished by mounting the set of five prints to a piece of chip board and placing them in the Fisher Scientific Isotemp Oven at a temperature of 140^{o} F (60^{o} C) for a period of 24 hours. The prints were then removed and a one-hour acclimation time occurred in which the print samples cooled, after which the ink testing procedures were conducted.

Freeze Condition (FC). The purpose of creating a freezing exposure condition was to subject the print samples to the environment that a package would endure in its lifecycle, whether through environments it would be exposed to in shipping as a secondary packaging application, or environments it would be exposed to as a primary packaging application. The environmental condition was simulated by placing the print samples in a Ziploc® brand freezer bag and placing them in the researcher's spare GE Spacemaker® 4.3.0 Cu. Ft. Compact Refrigerator/Freezer in the freezer compartment at a temperature of 15^{o} F (-9.4^{o} C) which met the conditions for freezing temperatures (32^{o} F or 0^{o} C). After a period of 24 hours, the print samples were removed from the freezer and a 1-hour acclimation period began. After this period, the print samples were subjected to ink testing procedures.

Vacuum Condition (VC). The purpose of creating a vacuum exposure condition was to subject the print samples to the environment that a package would endure in its lifecycle, whether through environments it would be exposed to in shipping as a secondary packaging application, or environments it would be exposed to as a primary packaging application. This condition was

created by sealing the five print samples in a Space Savers (Model 1AT91208 by Space Bag®) 13.75" x 19.5" storage bag for 24 hours. The vacuum seal was created by connecting a standard household upright vacuum to the valve. When the upright vacuum was turned on, the air within the bag was removed and a vacuum environment was created. After a period of 24 hours the print samples were removed from the vacuum-sealed bag and a one-hour acclimation period began. After this period, the print samples were subjected to ink testing procedures.

Rain Condition (RC). The purpose of creating a rain exposure condition was to subject the print samples to the environment that a package would endure in its lifecycle, whether through environments it would be exposed to in shipping as a secondary packaging application, or environments it would be exposed to as a primary packaging application. This condition was achieved by attaching the samples to a plastic backing board and standing this backing board up in a water basin. Tap water with a temperature of 45^{o} F (7.2^{o} C) was circulated through a sprinkler head attached to a half-inch plastic hose connected to a TEEL open-air submersible pump. The hose was suspended 12 inches above the backing board and directionally aimed so that the spray from the sprinkler head completely covered the prints. This was performed for a period of 24-four hours at which point the samples were removed and a one-hour acclimation period, in which the samples were allowed to air-dry, occurred. After this period, the print samples were subjected to the ink testing procedures.

Ink Testing Procedures

Several ink testing procedures have been established within the print industry to test the properties of inks under many common end-use conditions. These tests are used to evaluate ink requirements and performance under a given set of conditions[6]. The purpose of this experiment was to test the performance of a silver conductive water-based ink under certain common environmental conditions that flexible substrates, such as polyamides, could be subjected to. Therefore, five tests were selected: conductivity, density and color, adhesion, abrasion, and creasing.

Conductivity

A Model # 22-806 RadioShack digital multimeter was used to measure electrical resistance of the print samples. To determine the conductivity of the tint patches—the inverse measurement of conductivity—resistance was measured in ohms/square and was performed by measuring the resistance over a one-centimeter distance. Five different measurements were taken on various locations of each of the patches and were averaged. These averages were recorded for both the control and environmental conditions and compared.

Density and Color

Density and color was measured using an X-Rite DTP 22 Model handheld spectrophotometer. A spectrophotometer was the chosen measuring device because the researcher wanted to collect both density information as well as the color data of the ink. An average of five density and L*a*b* values were taken on each sample exposed to an environmental condition from various points on each tint patch and recorded.

These averages were then compared to those of the control sample, and the Delta E value for both the control and environmental condition were calculated and compared. The purpose of

calculating the Delta E value was to compare the change in color from the control sample to that of the environmentally exposed sample to determine if the exposure had an effect on the color of the ink.

Adhesion

The adhesion of the ink for both the control sample and the environmental condition sample were tested. The print samples were secured to the surface of a table. A piece of 1-inch by 2-inch pressure-sensitive tape (3M-610) was applied to the print sample. A rubber roller was used to ensure that there were no air bubbles between the tape and the substrate. The tape was then pulled from the print sample at a 150° angle, and the resistance of the sample was measured after each removal of the tape. The number of adhesive pulls it took to cause conductivity failure was recorded. The average of these values was compared with the average of the control set to determine whether exposure to a certain environmental condition had an effect on the adhesion performance of the ink.

Abrasion

Abrasion testing was performed in the fashion of the Sutherland rub test that has been established as a standard for testing ink adhesion of flexographic inks. The purpose of this test was to make sure that an antenna printed on a package could withstand handling between the press and point of sale, which includes typical shipping environments[6]. This was performed by attaching the print sample print-side up to an inclined plane at a 20° angle. A piece of nylon substrate was attached to the bottom of a 500 g weight that was released at the top of the inclined plane 10 times after which a measurement of resistance was taken of each tint patch. This was repeated until the tint patch exhibited an infinite measurement of resistance. This indicated that the patch was no longer conductive. The number of passes it took to achieve this status for each patch of the environmental condition sample was recorded and compared to the number recorded for the control condition.

Creasing

Crease testing was conducted by making a crease on each of the tint patches. Each crease was made by folding the print sample once and placing a weight on it for a period of 10 minutes. The resistance was measured and recorded. Each tint patch of the print sample was then unfolded/refolded with the weight replaced on the sample for 10 minutes until the measurement of the patch indicated conductivity failure. The number of times the samples were creased was recorded for both the control and the environmental condition sample. The average of these values was compared to determine if the environmental exposure had an effect on the integrity of the ink.

Data Analysis

A simple statistics model was used in evaluation of the data set. Averages of results for each print sample of the individual environmental conditions were calculated for each of the tests performed. These calculations were then compared to that of the control environment to analyze the results.

Limitations

One of the limitations of this experiment was that a limited number of samples were tested. For the testing used in this experiment to be statistically significant, a minimum of 1,200 print samples should be tested. 60 samples (30 control, 30 exposure) per the four environmental conditions per the five ink tests is the minimum desired sample size for statistical significance (60 prints * 4 environmental conditions * 5 ink tests = 1,200 total prints). Testing of this scale was not possible because of the limitations of the scope of this project.

Another limitation was that the environmental conditions that were set up for this experiment are simulations of a real-world environment. Results would be more accurate if the experiment was tested over a period of time in the actual environments described.

Results

Treatment of Control Sets

For each ink-testing procedure performed, a comparison control set was printed for each of the four environmental conditions. In addition to comparison against the set of prints exposed to the environmental conditions, the consecutive control sets (#1–4) were compared to each other. The reason for comparing control sets is because of inconsistent measurements particularly for the 80–70% tint patches. The significant results (Figures 2 – 4) of this comparison of consecutive controls sets for particular ink tests that showed discrepancy are indicated in the following figures.

Discussion of Treatment of Control Sets

Conductivity. In Figure 2, the resistance measured in ohms/cm was compared between control sets #1–4 for each of the tint patches. In comparison of these measurements, it can be seen that each successive control set provided more resistance than the previous.

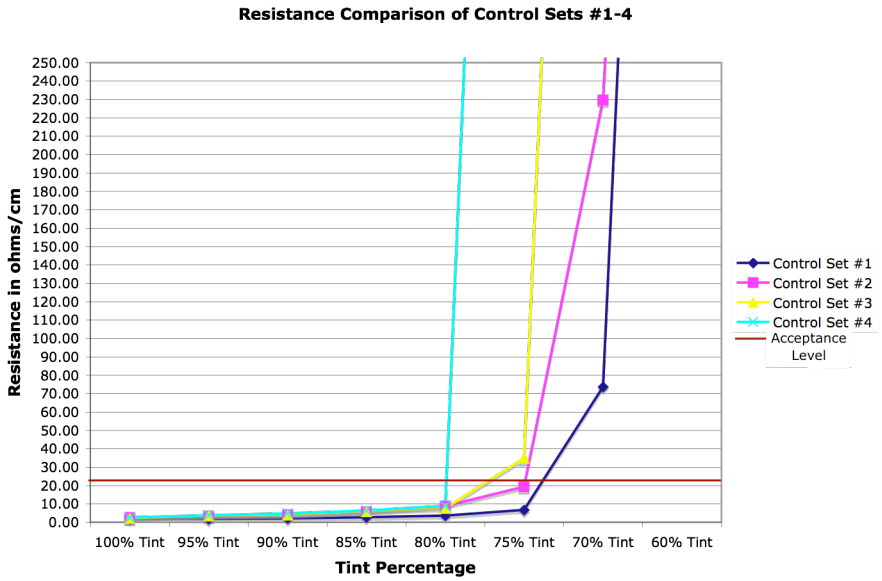

Figure 2. Resistance Comparison of Control Set #1-4

Density. In Figure 3, the density measurement was compared between control sets #1–4 samples for each of the tint patches. This graph indicates that the control set density measurements differed by 0.021 for the 75% and 70% tint patch and 0.038 for the 60% tint patch.

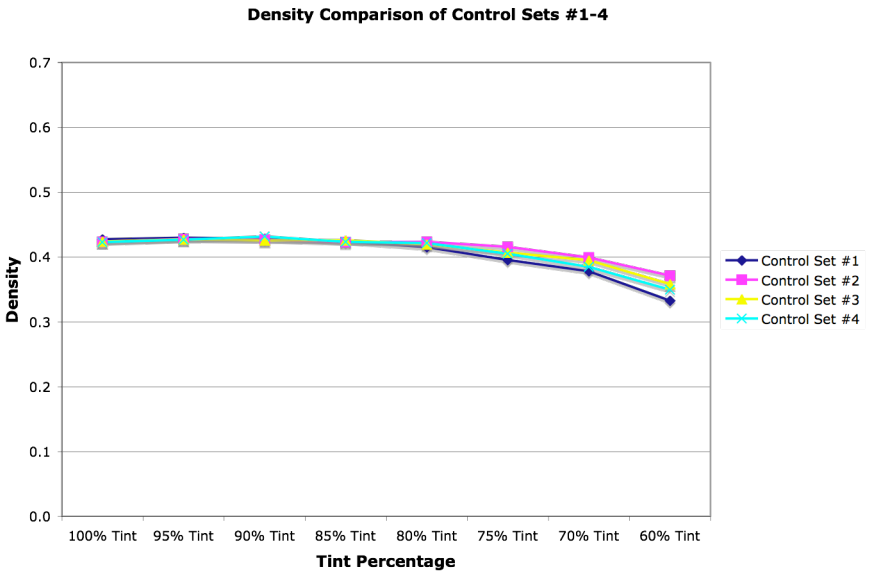

Figure 3. Density Comparison of Control Sets #1-4

Adhesion. Figure 4 shows the adhesion of control sets #1–4. The number of passes is indicated on the x-axis, the tint percentage value is indicated on the y-axis and the measurement of resistance in ohms/cm is indicated on the z-axis. The apex of the surface graph for each patch indicates the highest resistance measurement achieved. The decline of the graph that follows the peak is the number of passes where a failure of conductivity occurred resulting in a null measurement. The red box indicates the level of resistance permitted for use in production of an RFID antenna (25 ohms/square). Any measurement below this level passes for acceptable conductivity of the ink. Each successive control set performed more poorly than the preceding. Control Set #1 conductivity dropped off after two passes on the 70% tint patch; Control Set #2 dropped off after three passes on the 80% tint patch; Control Set #3 dropped off after three passes on the 80% tint patch also but recorded much higher resistance levels than that of Control Set #2. Control Set #4 dropped off after two passes on the 85% tint patch. This indicates that there was a negative effect on the successive print performances of each control set.

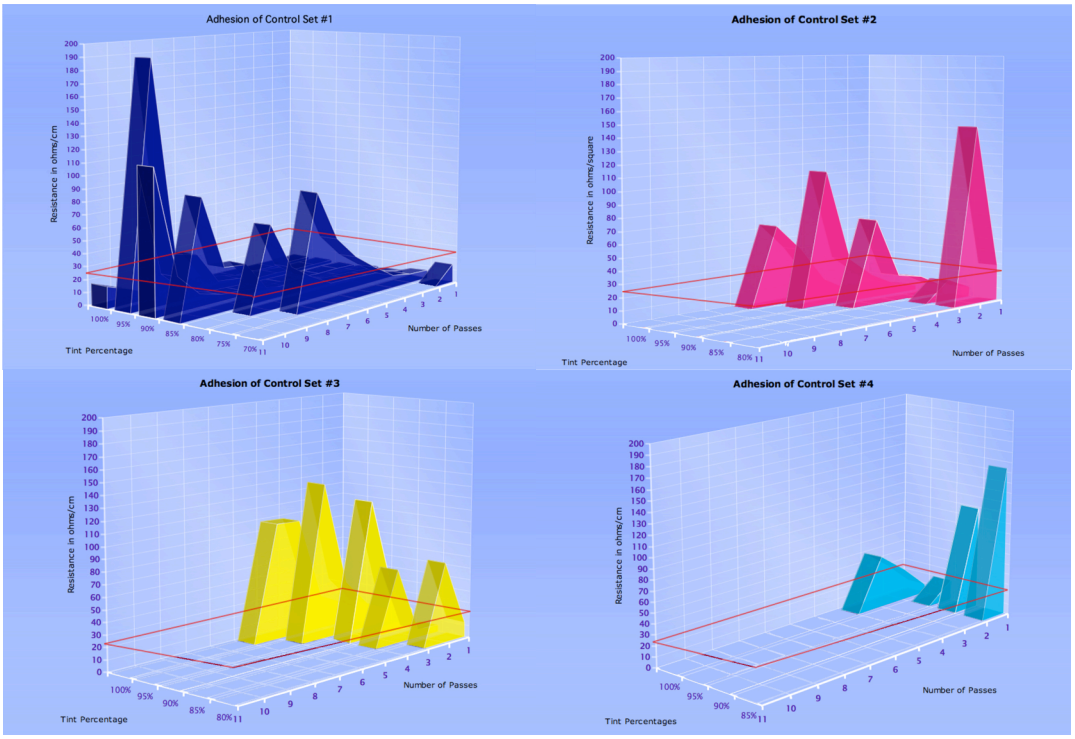

Figure 4. Adhesion Comparison of Control Sets #1-4

Test A – Conductivity

The conductivity test was performed using a digital multimeter on which measurements of resistance were recorded in ohms/square, five times at five different points on the each of the tint patches (100-95-90-85-80-75-70-60). The means of the measurements (Figures 5-7) were then calculated and the significant results were graphed.

Discussion of Conductivity

Heat Condition. In Figure 5, the resistance measured in ohms/cm was compared between the Control Set #1 and Heat Set samples for each of the tint patches. This comparison provides several indications. For the Control Set, it can be seen that the conductivity level dropped off after the 70% tint patch. The Heat Set conductivity dropped off at the 80% tint patch. The measurements for the 100% patch through the 85% patch appeared to be uneffected by exposure the environmental condition. The conductivity level of the samples exposed to the Heat Condition appeared to be uneffected for the 100–85% tint percentage; however the conductivity level was definitely effected by exposure to the condition for the 80–70% patches. For both, the 60% patch measured a greater resistance to conductivity than permitted by the acceptable level for antenna production previously established.

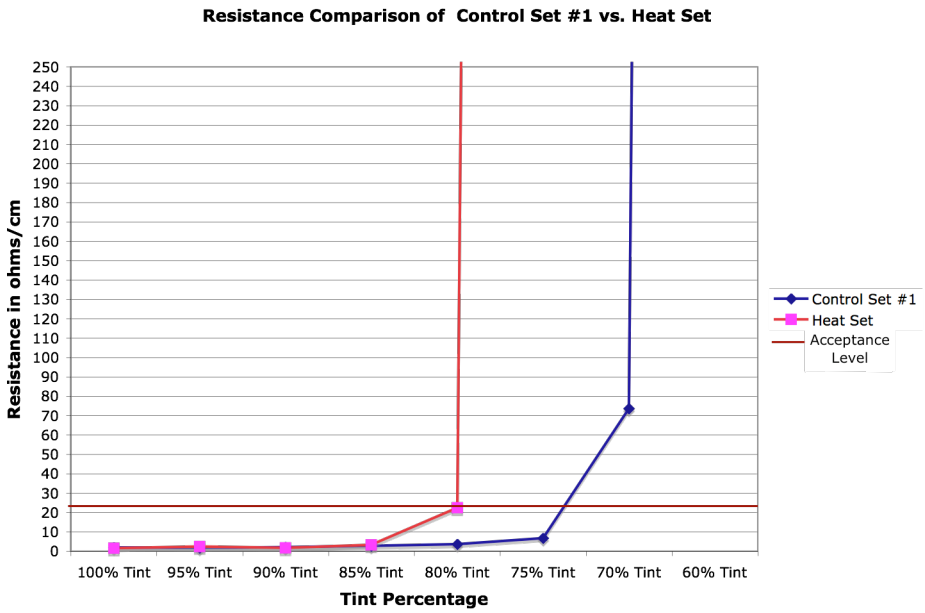

Figure 5. Resistance Comparison of Control Set #1 vs. Heat Set

Freeze Condition. In Figure 6, the resistance measured in ohms/cm was compared between the Control Set #2 and Freeze Set samples for each of the tint patches. The Control Set conductivity level dropped off after the level of the 70% tint, which is consistent with the measurement from Control Set #1. The Freeze Set sample conductivity also dropped off after the 70% tint level, however the resistance measurement for the Freeze Set at the 70% tint level was 36.22 ohms/cm. The Control Set measurement is 229.70 ohms/cm at this level. This indicates that exposure to the freeze condition appeared to slightly improve the conductivity for the 80–70% tint. Consistent with the results of Control Set #1, the 60% tint patch was not conductive.

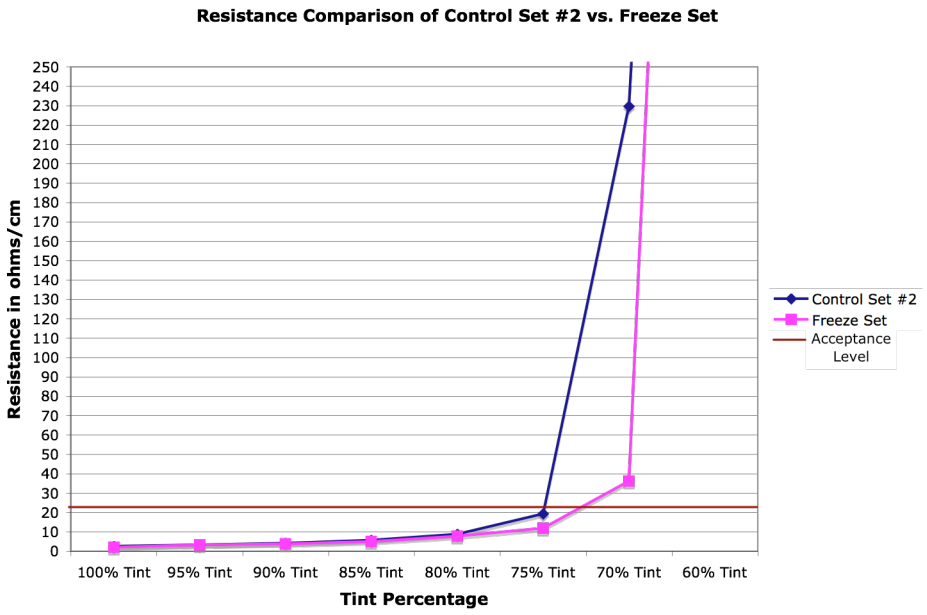

Figure 6. Resistance Comparison of Control Set #2 vs. Freeze Set

Rain Condition. In Figure 7, the resistance measured in ohms/cm was compared between the Control Set #4 and Rain Set samples for each of the tint patches. Both the Control Set and the Rain Set samples dropped off in conductivity level after the 80% tint patches. The 100–80% tint patches all produced a resistance measurement that was significantly higher than that of the Control Set, indicating that exposure to the Rain Condition had an effect on the conductivity level of the print samples.

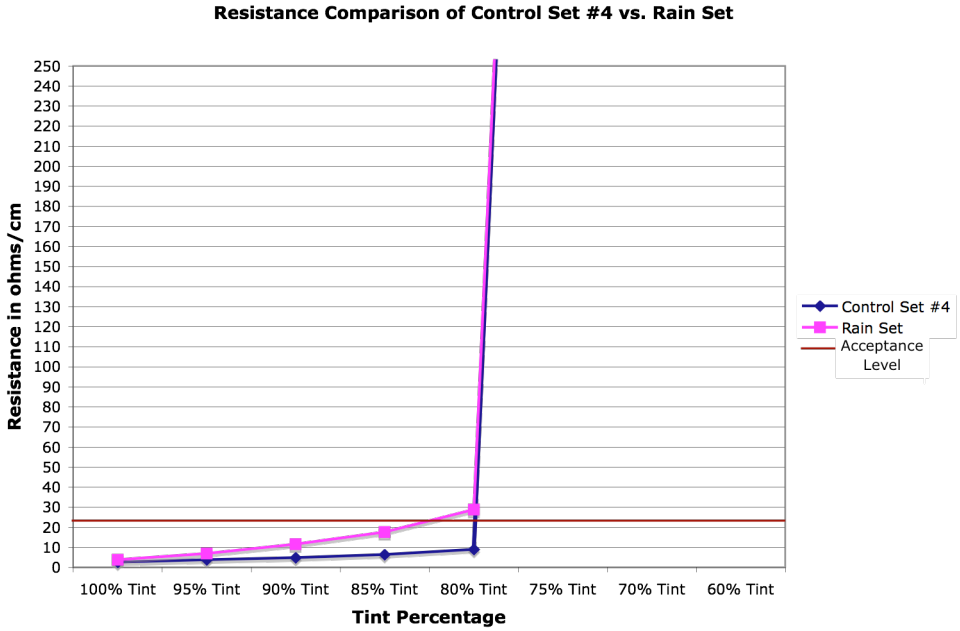

Figure 7. Resistance Comparison of Control Set #4 vs. Rain Set

Test B – Density and Color

Density Test

The density test was performed using a handheld spectrodensitometer in which measurements were taken five times at five different points on the each of the tint patches (100-95-90-85-80-75-70-60). The means of the measurements were then calculated and graphed (Figures 27–30).

Discussion of Density

Heat Condition. In Figure 8, the density measurement was compared between the Control Set #1 and Heat Set samples for each of the tint patches. For every tint patch 100–60%, the density measurements of the Heat Set are higher than those of the Control Set. This indicates that exposure to the heat condition does have an effect on the density of the print samples.

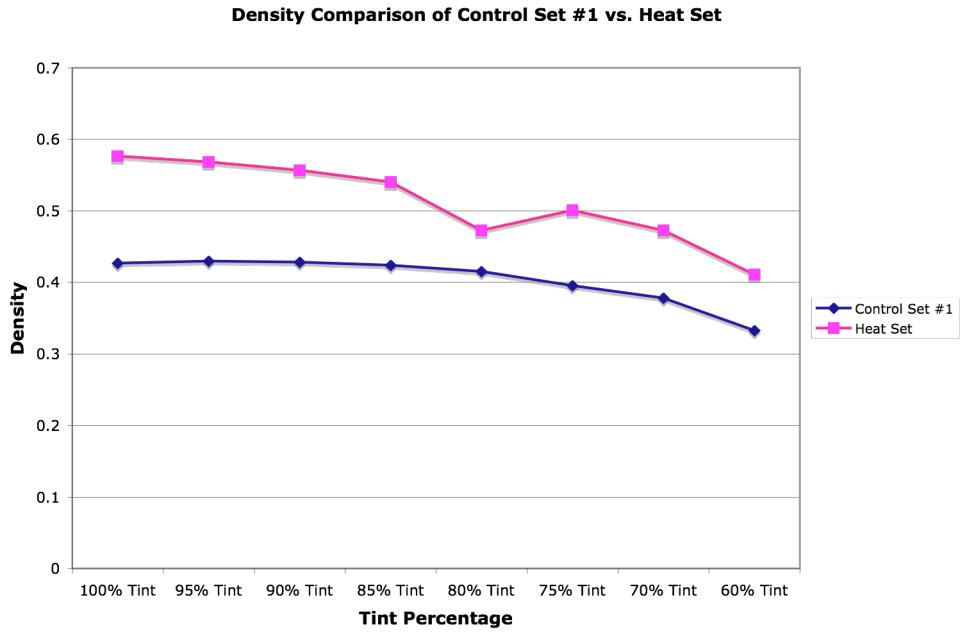

Figure 8. Density Comparison of Control Set #1 vs. Heat Set

Color Test

The color test was performed using a handheld spectrodensitometer in which measurements were taken five times at five different points on the each of the tint patches (100-95-90-85-80-75-70-60). The means of the measurements were then calculated and the significant results are represented in Figures 9–10.

Discussion of Color Test

Heat Condition. In Figure 9, the L* values indicate that there was a significant shift in lightness from the Control Set to the Heat Set. The a*, b* values indicated that there was a significant shift in the color space of the Heat Set ink to a more blue (b* axis) and red (a* axis) hue than that of the Control Set. This indicates that exposure to the heat condition produced a significant shift in L*a*b* values.

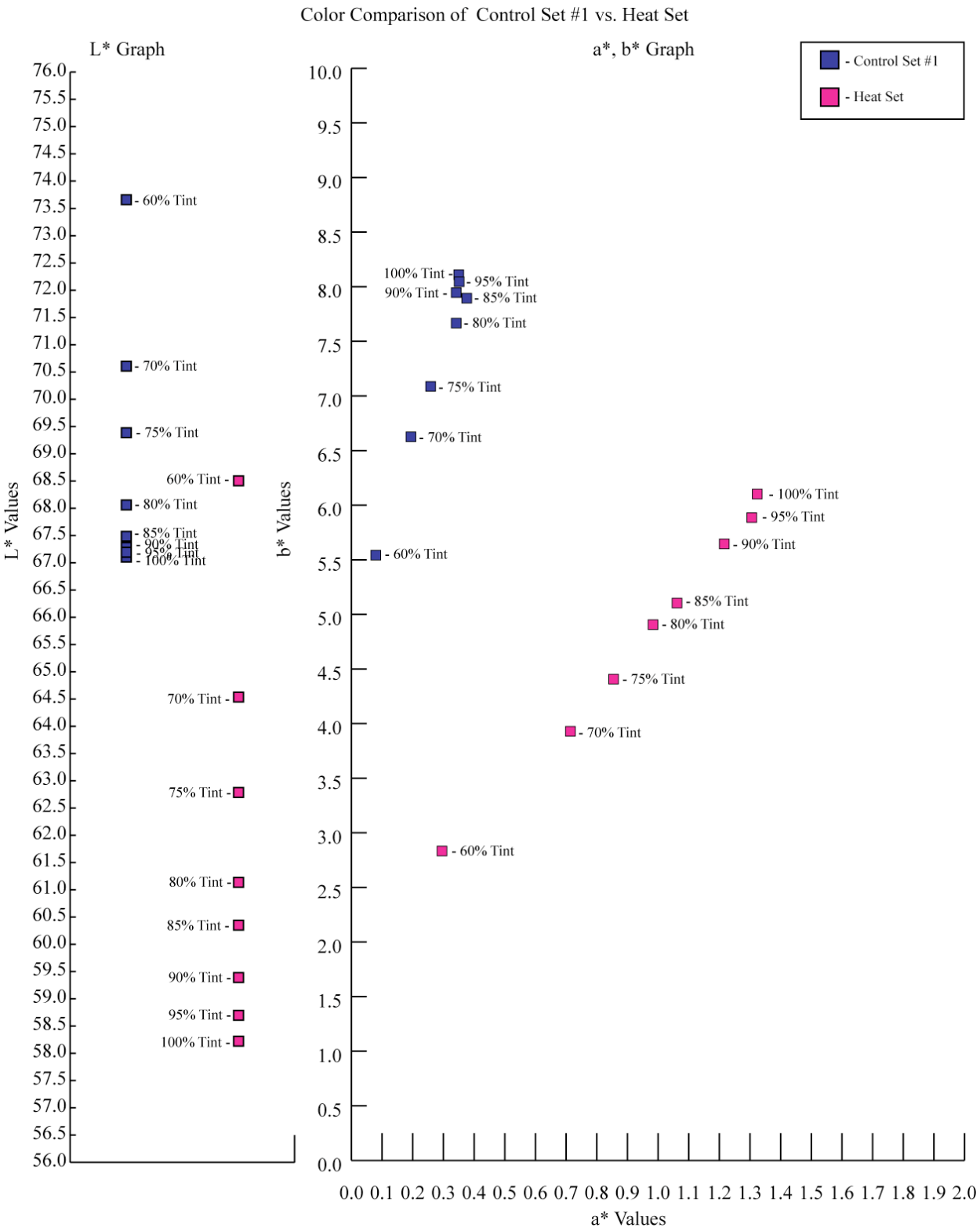

Figure 9. L* and a*, b* Comparison of Control Set #1 vs. Heat Set

Rain Condition. In Figure 10, the L* values indicate that there a slight shift in lightness of the Rain Set. Also, the a*, b* values have shown that there was a slight shift in the color space of the

Rain Set. This indicates that the rain condition has a slight effect on the color of the print samples.

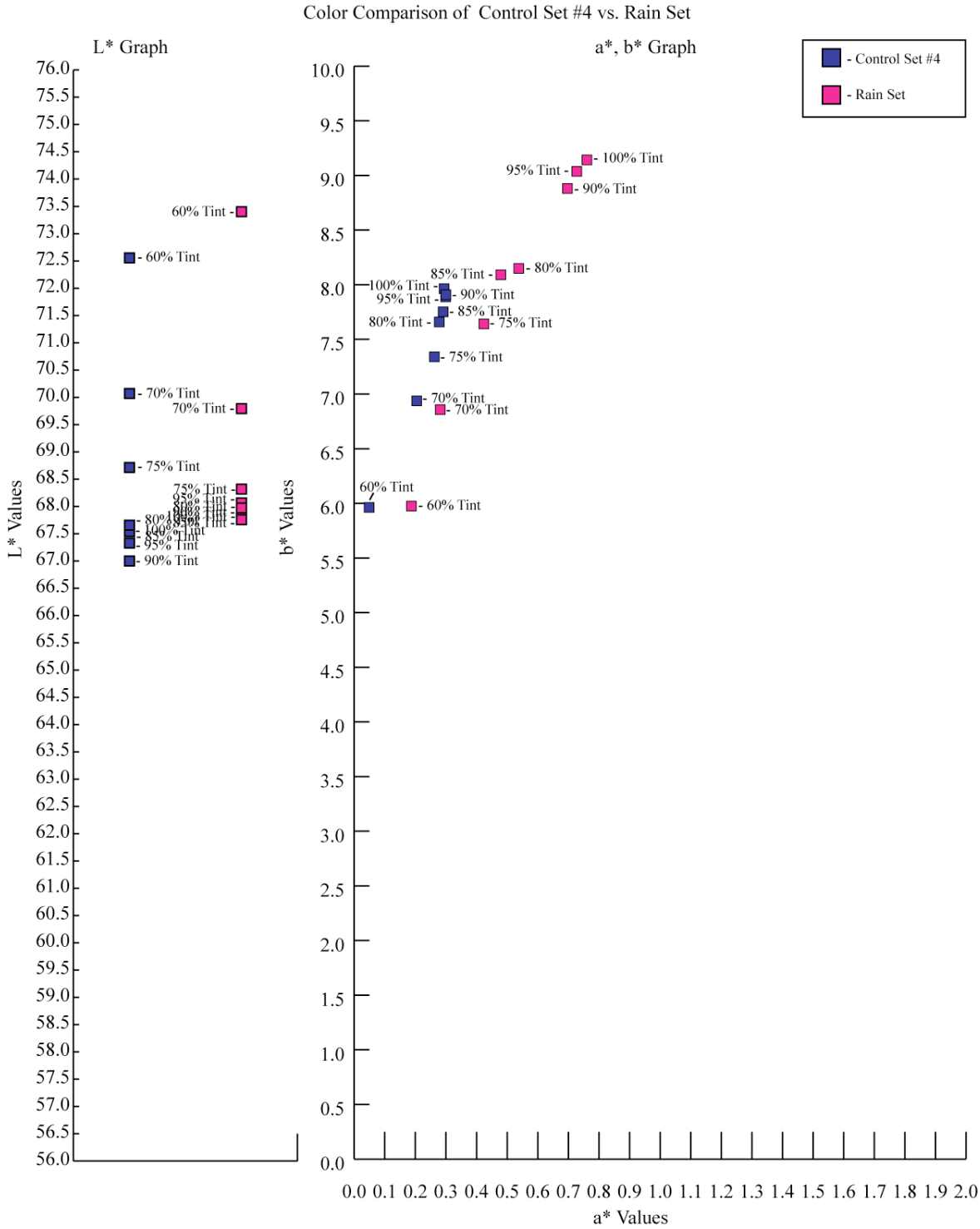

Figure 10. L* and a*, b* Comparison of Control Set #4 vs. Rain Set

Delta E Comparison

Table 2 shows the change in color for the control sets and their respective environmental conditions for each tint percentage patch. This table indicates that the greatest difference in color was produced by exposure to the heat condition. Most of the Delta E measurements for all of the conditions fall within the commonly accepted level of a Delta E value of 4–8 that is used in print production[4].

Tint Percentage	CS #1 and HS Delta E	CS #2 and FS Delta E	CS #3 and VS Delta E	CS #4 and RS Delta E
100%	9.331	0.114	0.219	1.298
95%	8.730	0.310	0.084	1.431
90%	8.140	0.443	0.130	1.365
85%	7.691	1.187	2.135	0.444
80%	7.482	2.095	0.138	0.637
75%	7.147	1.533	0.182	0.524
70%	6.664	1.490	1.655	0.370
60%	5.762	2.143	0.694	0.857

Table 2. Delta E values for Control Sets vs. Environmental Condition Sets

Test C– Adhesion

The adhesion test was performed using the pressure sensitive tape adhesion testing previously described. The number of passes it took to cause the sample to provide an infinite resistance measurement was recorded, and the mean of these values for both the environmental set and control set were graphed (Figures 11–14) to determine whether exposure to a certain environmental condition had an effect on the ink of the printed sample.

Discussion of Adhesion

Heat Condition. Figure 11 compares the adhesion of Control Set #1 and the Heat Set. The number of passes is indicated on the x-axis, the tint percentage value is indicated on the y-axis and the measurement of resistance in ohms/cm is indicated on the z-axis. The apex of the surface graph for each patch indicates the highest resistance measurement achieved. The decline of the graph that follows the peak is the number of passes where a failure of conductivity occurred resulting in a null measurement. The red box indicates the acceptable level of resistance permitted for use in production of an RFID antenna (25 ohms/square). Any measurement below this level passes for acceptable conductivity of the ink. The conductivity of the Heat Set dropped off after the 90% tint patch, while the Control Set dropped off after the 70% tint patch. Also, the number of passes it took to break the conductivity of the Heat Set was significantly less than that of the Control Set. This shows that the heat condition had a negative effect on the adhesion properties of the print samples when compared to the Control Set.

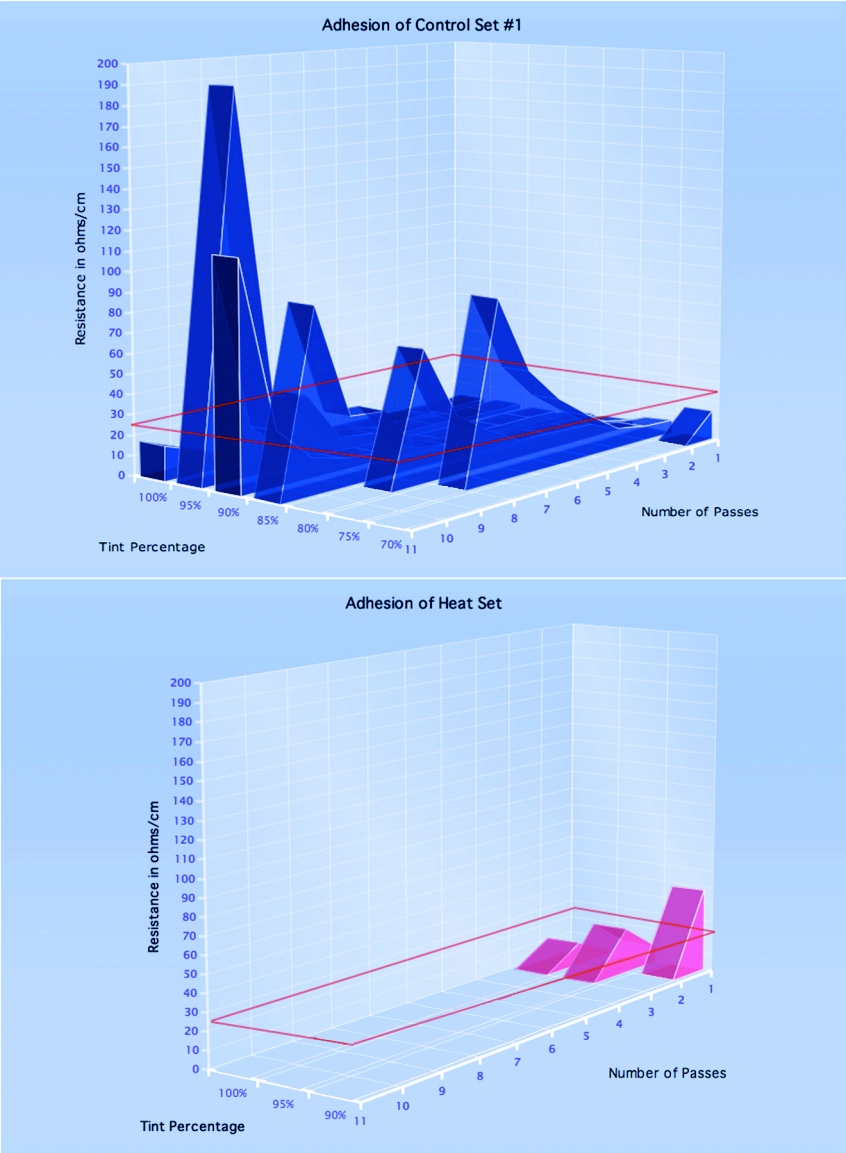

Figure 11. Adhesion Comparison of Control Set #1 vs. Heat Set

Freeze Condition. Figure 12 compares the adhesion of Control Set #2 and the Freeze Set. The number of passes is indicated on the x-axis, the tint percentage value is indicated on the y-axis and the measurement of resistance in ohms/cm is indicated on the z-axis. The apex of the surface graph for each patch indicates the highest resistance measurement achieved. The decline of the graph that follows the peak is the number of passes where a failure of conductivity occurred resulting in a null measurement. The red box indicates the acceptable level of resistance permitted for use in production of an RFID antenna (25 ohms/square). Any measurement below this level passes for acceptable conductivity of the ink. The conductivity of the Freeze Set dropped off after the 75% tint patch, while the Control Set dropped off after the 80% tint patch. Also, the number of passes it took to break the conductivity of the Freeze Set was more than that of the Control Set. This shows that the freeze condition had a positive effect on the adhesion properties of the print samples when compared to the Control Set.

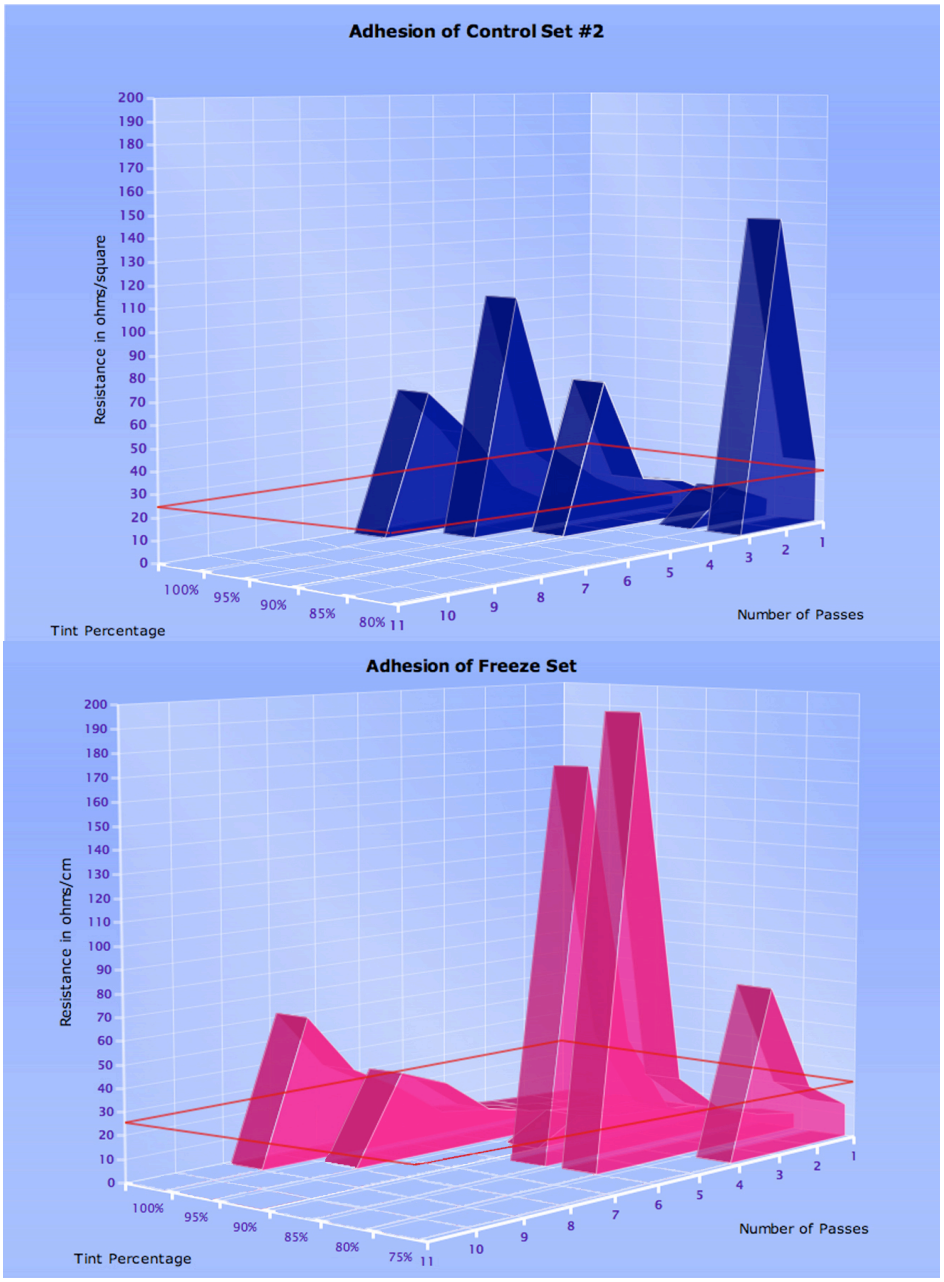

Figure 12. Adhesion Comparison of Control Set #2 vs. Freeze Set

Vacuum Condition. Figure 13 compares the adhesion of Control Set #3 and the Vacuum Set. The number of passes is indicated on the x-axis, the tint percentage value is indicated on the y-axis and the measurement of resistance in ohms/cm is indicated on the z-axis. The apex of the surface graph for each patch indicates the highest resistance measurement achieved. The decline of the graph that follows the peak is the number of passes where a failure of conductivity occurred resulting in a null measurement. The red
box indicates the acceptable level of resistance permitted for use in production of an RFID antenna (25 ohms/square). Any measurement below this level passes for acceptable conductivity of the ink. The conductivity of the Vacuum Set dropped off after the 85% tint patch while the Control Set dropped off after the 80% tint patch. Also, the number of passes it took to break the

conductivity of the Vacuum Set was less than that of the Control Set. This shows that the vacuum condition had a negative effect on the adhesion properties of the print samples when compared to the Control Set.

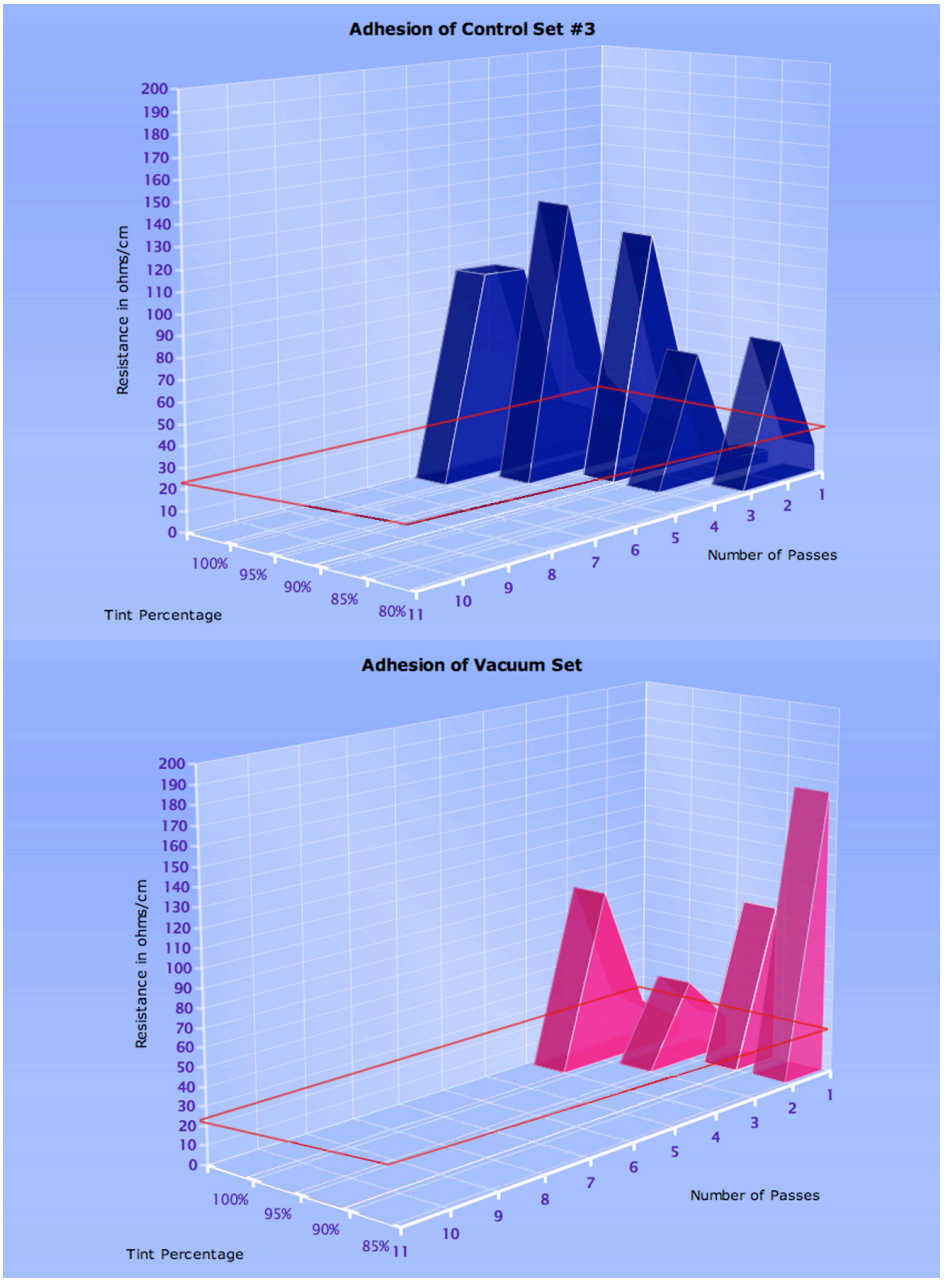

Figure 13. Adhesion Comparison of Control Set #3 vs. Vacuum Set

Rain Condition. Figure 14 shows the adhesion of Control Set #4. The number of passes is indicated on the x-axis, the tint percentage value is indicated on the y-axis and the measurement of resistance in ohms/cm is indicated on the z-axis. The apex of the surface graph for each patch indicates the highest resistance measurement achieved. The decline of the graph that follows the peak is the number of passes where a failure of conductivity occurred resulting in a null measurement. The red box indicates the acceptable level of resistance permitted for use in

production of an RFID antenna (25 ohms/square). Any measurement below this level passes for acceptable conductivity of the ink. The Rain Set that is being compared to this Control Set is not graphed because the conductivity level broke on each tint patch after only one pass, resulting in infinite resistance for each measurement. The conductivity of the Control Set dropped off after the 85% tint patch, and the number of passes it took to break the conductivity of the Rain Set was significantly less than that of the Control Set. This shows that the rain condition had a severe negative effect on the adhesion properties of the print samples when compared to the Control Set.

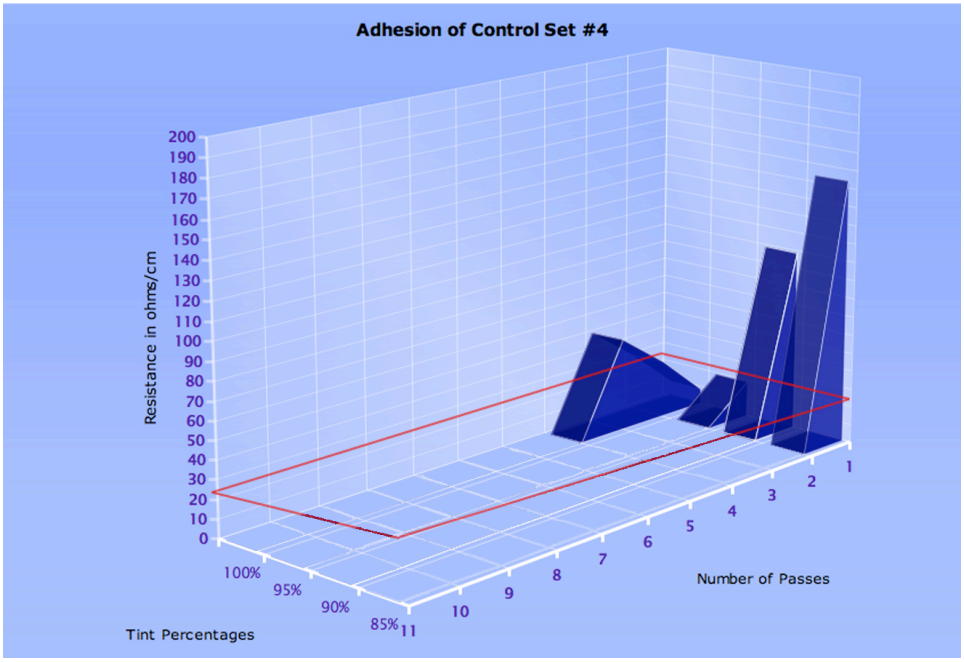

Figure 14. Adhesion Comparison of Control Set #4

Test D – Abrasion

The abrasion test was performed by attaching the print samples, print side up, to a surface inclined at a 20° angle. A piece of nylon substrate was attached to the bottom of a 500 g weight, and the weight was released at the top of the inclined block 10 times. A measurement of resistance was taken for each tint patch. This was repeated until the tint patch exhibited a measurement of infinite resistance, which indicated that the patch was no longer conductive. The number of passes it took to achieve this status for each patch of both the environmental set and control set sample was recorded and compared (Figures 15–16).

Discussion of Abrasion

Vacuum Condition. Figure 15 shows the abrasion of Control Set #3 and the Vacuum Set. The number of passes is indicated on the x-axis, the tint percentage value is indicated on the y-axis and the measurement of resistance in ohms/cm is indicated on the z-axis. The apex of the surface graph for each patch indicates the highest resistance measurement achieved. The decline of the graph that follows the peak is the number of passes where a failure of conductivity occurred resulting in a null measurement. The red box indicates the acceptable level of resistance permitted for use in production of an RFID antenna (25 ohms/square). Any measurement below this level passes for acceptable conductivity of the ink. The conductivity level of Control Set #3

dropped off after 10 passes at the 75% tint patch. The conductivity level of the Vacuum Set dropped off after 60 passes at the 85% tint patch. This indicates that there was a difference in resistance measurements between Control Set #3 and the Vacuum Set. In this test, exposure to the vacuum condition had a negative impact on the abrasion resistance properties of the print samples.

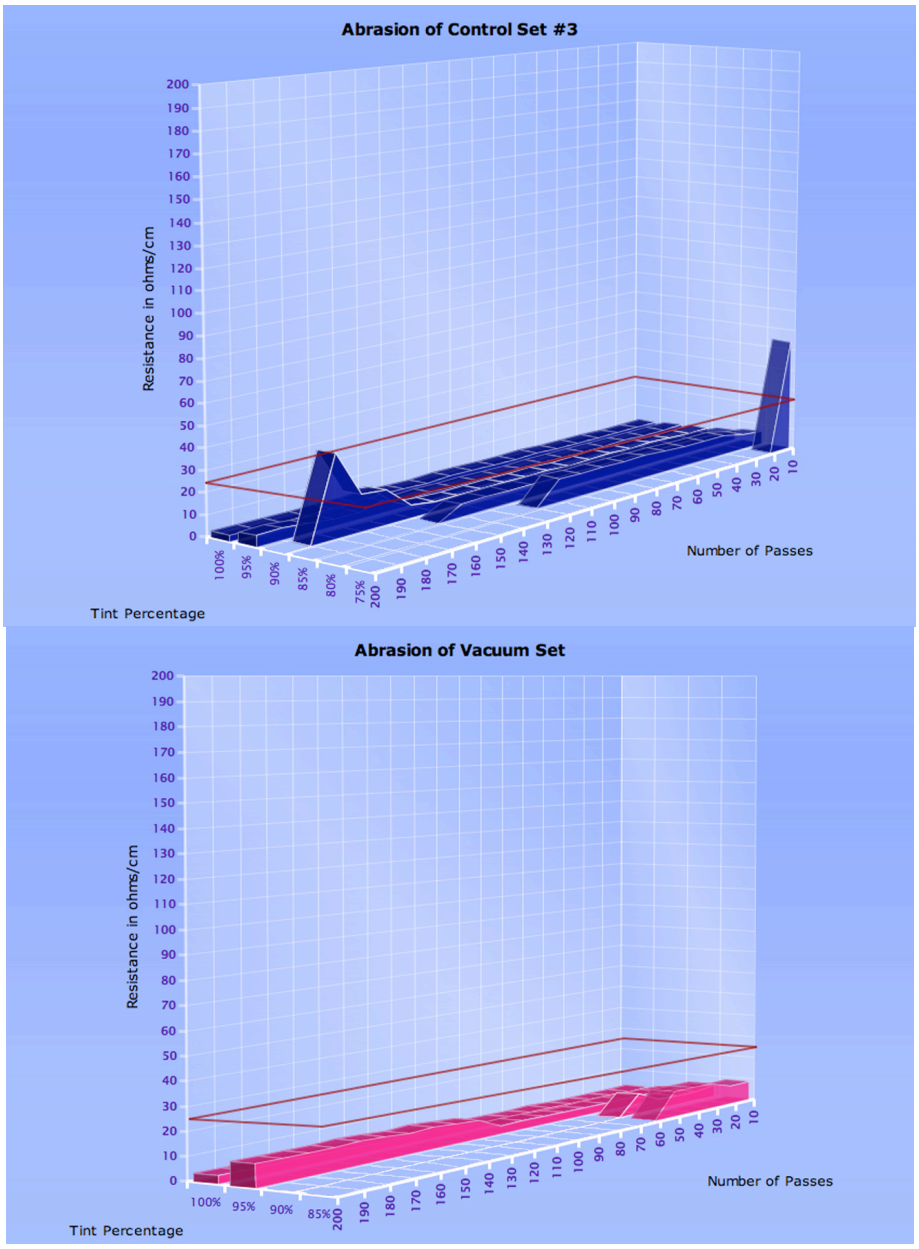

Figure 15. Abrasion Comparison of Control Set #3 vs. Vacuum Set

Rain Condition. Figure 16 shows the abrasion of Control Set #4 and the Rain Set. The number of passes is indicated on the x-axis, the tint percentage value is indicated on the y-axis and the measurement of resistance in ohms/cm is indicated on the z-axis. The apex of the surface graph for each patch indicates the highest resistance measurement achieved. The decline of the graph that follows the peak is the number of passes where a failure of conductivity occurred resulting

in a null measurement. The red box indicates the acceptable level of resistance permitted for use in production of an RFID antenna (25 ohms/square). Any measurement below this level passes for acceptable conductivity of the ink. The conductivity level of Control Set #4 dropped off after 40 passes at the 75% tint patch. The conductivity level of the Rain Set dropped off after 40 passes at the 80% tint patch. This indicates that there was a slight difference in resistance measurements between Control Set #4 and the Rain Set. In this test, exposure to the rain condition had a negative impact on the abrasion resistance properties of the print samples.

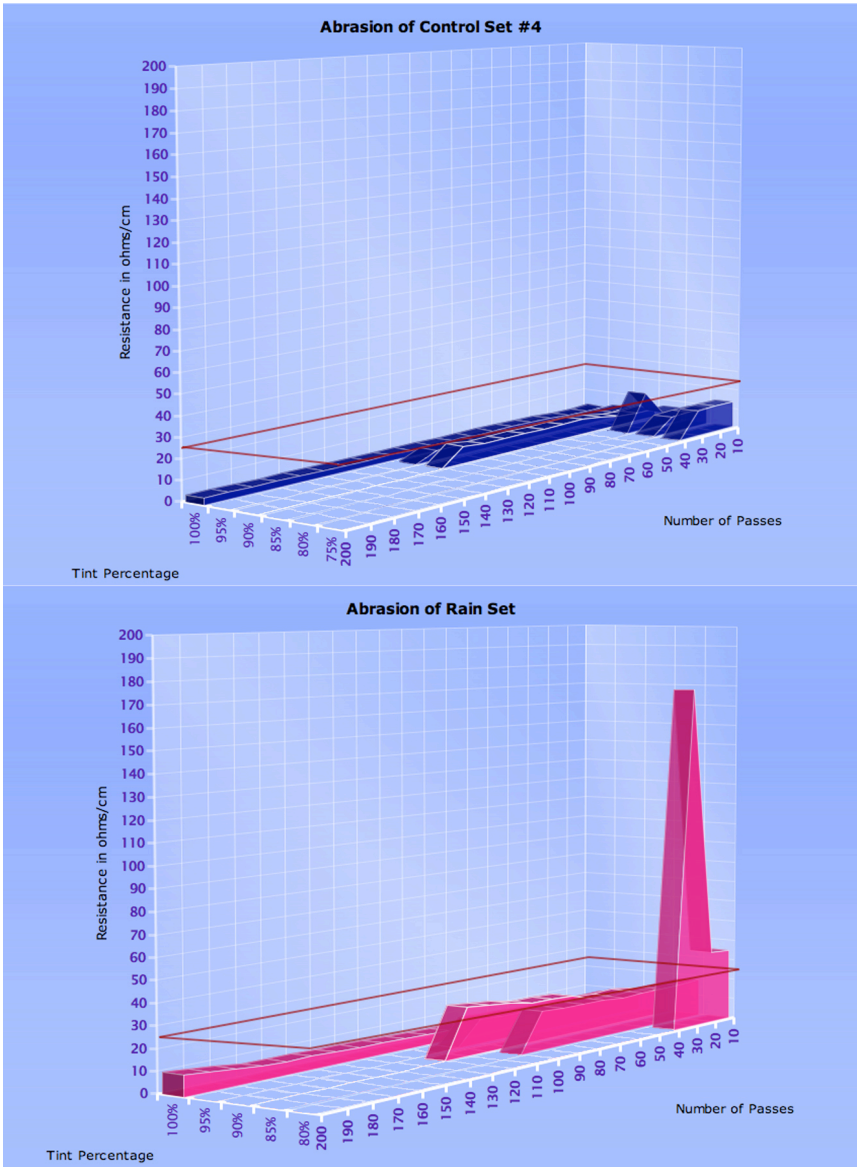

Figure 16. Abrasion Comparison of Control Set #4 vs. Rain Set

Test E – Creasing

In each of the four control and environmental condition trials of this test, creasing each tint patch once caused an absolute resistance measurement. This indicates that any creasing of the print

samples will cause infinite resistance. No determination can be made regarding the effect of any of environmental conditions on the creasing properties of the print samples. However, it can be determined that creasing any printed sample using the test ink and substrate will cause the conductivity of the print sample to break, thus rendering it ineffective.

Determination of Acceptable Ink Film Thickness

Caliper was used to measure an ink film thickness level that is acceptable for printed RFID antenna production. The thickness of the substrate was determined to be 0.2 mils. The thickness of each tint patch printed on the substrate was found and then the substrate thickness of 0.2 mils was subtracted to determine the ink film thickness (Table 3).

Tint Percentage	Ink Density Level
100%	1.1 mils
95%	1 mils
90%	0.7 mils
85%	0.5 mils
80%	0.4 mils
75%	0.3 mils
70%	0.1 mils
60%	< 0.1 mils

Table 3. Ink density level of print sample by tint percentage

A functional printed RFID antenna was measured to be 0.2 mils. This measurement was then established as the minimum acceptable ink film thickness for the purpose of this study.

Summary and Conclusions

Environmental variables tested did not have an effect on the performance quality of silver RFID water-based flexographic ink when printed on a polyamide substrate for the 85–100% ink density levels. Environmental variables may have an effect on the performance quality of RFID water-based flexographic ink when printed on a polyamide substrate for the 70–80% ink density levels. The 100–75% tint patch ink density levels were deemed acceptable for use in production of RFID antennas because they meet the acceptable solid ink density level of 0.2 mils or greater for RFID antenna production. Although some effects of environmental exposure were observed for the 75% tint and below, these ink film thickness are unlikely to be printed in commercial production.

Heat Set

Effects of the heat condition were apparent in the 70–80% tint patches for all ink tests except for the abrasion and crease tests. For the conductivity test, the heat condition effected the print sample by causing a rise in resistance levels of the ink.

Effects of the heat condition can also be seen in a change in density with increasing temperature. This is likely because heat application caused more complete ink film curing. Increased curing may result in a reduction of the amount of polymers present in the ink retaining matrix. This reduction will allow the silver particles to come more into contact.

It was anticipated that heat curing would have a positive effect on adhesion and abrasion resistance. Adhesion, however, was negatively impacted. Poor adhesion may have been the result of dimensional changes in the nylon with the application of heat. These dimensional changes would weaken the interfacial bond between the ink and substrate. There was not a significant impact on abrasion resistance of the sample.

The heat condition also caused a shift in color of the print sample. The heat set print sample produced L* values that were darker than that of the Control Set and the a*, b* values of the heat sample shift to more red values on the a* axis and more blue values on b* axis. The Delta E measurements calculated for all of the tint patches range from 5.67 to 9.33. The acceptable Delta E value in press environments ranges from 4 to 8. Therefore, the range that the Heat Set sample produced was still relatively within the acceptable range.

Freeze and Vacuum Set
Exposure to the freeze and vacuum conditions did not have a significant enough impact to indicate an effect on the print performance.

Rain Set
The rain condition exhibited some effect on the adhesion and abrasion properties of the print samples. Conductivity was lost after only one pass. After exposure to water the ink film was completely removed by the tape. The condition was also the only environmental variable to exhibit an impact on the abrasion resistance of the samples.

All effects on performance of the sample are likely due to the fact that this substrate is particularly hydrophilic and probably absorbed a significant amount of moisture from exposure to this condition. This absorption of water caused poor bonding between ink and substrate. It was determined that in a production environment some sort of coating or lamination would perhaps improve this problem. This factor could, however, have a negative effect on the conductivity of the sample.

Control Sets
The ink test results from comparing Control Sets #1–4 with the exception of color and abrasion indicated the ink itself has a negative effect on the performance of the print sample. The ink was very abrasive to the proofing press. It caused the cells of the anilox plate to plug up quickly even when cleaning was performed after each print sample was created. The ink corroded the plate and damaged the stereo roller of the press.

Lastly, the ink had shear thickening properties that caused many of the print samples to have a marred image that was not acceptable for use in testing procedures. Metallic particles in the ink are large and became concentrated at the point of the printing process where the doctor blade meters the ink onto the impression roller, thus, causing a marred image. To correct this problem, careful observation of printing conditions was required and adjustments of the speed of the press were implemented.

Creasing Test

It was determined that creasing any antenna printed using this ink and substrate would render the antenna ineffective. Therefore, it appears that creasing has a negative impact regardless of exposure to environmental variables.

Summary

The 85–100% solid ink density levels of silver RFID water-based flexographic ink when printed on a polyamide substrate are not effected by exposure to environmental conditions of this study and therefore are acceptable for use in production of printed RFID antennas. This is important because the ink density level is likely to be printed at 100%. This study would then show that use of this ink with a polyamide substrate similar to nylon 6,6 would be acceptable for print production.

Agenda for Further Research

Due to the scope of this project, sample size was limited to 40 prints with each ink testing procedure only conducted once. It is possible that a change in results would be seen by performing the same type of experiment with a larger sample size over an extended period of time. For the scope of this study, a flexographic proofer was used to create the print samples. An interesting way to increase the sample size for an experiment like this would be to use a commercial flexographic press capable of producing more prints that would allow for the use of a printing plate that is imaged with a functional antenna design. The results of a study conducted in this manner would more appropriately reflect the behavior of the ink and the substrate in a real-world application.

Also, to simulate a more realistic environment, the parameters of this study could be extended to test a fully formed package design that has completed the finishing and filling processes required before the product enters the packaging distribution system.

To build off of this idea, the package could be tested after it has been exposed to the different environmental conditions over a longer time frame. This study only examined the performance of the ink over a 24-hour time frame. It is likely that the results would show more variability in ink performance if exposed to an environmental condition for perhaps a week or even over a year.

Finally, a way to extend the implications of the study to include a broader range of audience would be to include not only standard ink testing procedures but also standard package performance testing as well.

Acknowledgements

The researcher would like to thank Dr. Scott Williams and Deanna Jacobs for their direction and support during the research and compilation of this report. Dr. Scott Williams served as a thesis advisor and is an Associate Professor at the RIT School of Print Media. Deanna Jacobs, an Associate Professor at the RIT American Packaging Center for Plastics and Packaging Innovation, also served as a thesis advisor. The author would like to recognize their contributions to this project.

References

[1] Harrop, P. (2006, August 19). *Item level RFID—The prosperous market 2006–2016*. Retrieved September/October 2006, from http://www.idtechex.com/products/en/articles/00000485.asp

[2] Collins, J. (2003, October 16). Proposed standard for ink antennas. *RFID Journal*. Retrieved September, 2006, from http://www.rfidjournal.com/article/articleview/614/1/1

[3] Allcock, H. R., Lampe, F. W., & Mark, J. E. (Eds.). (2003). *Contemporary polymer chemistry* (3rd ed.). Upper Saddle River, NJ: Pearson Education. (Original work published 1981)

[4] Sharma, A. (2004). *Understanding color management*. New York: Thomson Delmar Learning.

[5] Chaplin, M. (2006, September 10). Rheology primer for hydrocolloid science. In *Water structure and behavior*. Retrieved March 15, 2007, from London South Bank University Web site: http://www.lsbu.ac.uk/water/hyrhe.html

[6] Foundation of Flexographic Technical Association. (1999). *Flexography: Principles & practices* (5th ed., Vols. 1–6). Ronkonkoma, NY: Foundation of Flexographic Technical Association.

[7] Vainstein, J. (2005). *A study of the condition and variables that affect the printing of shrink films on waterbased flexography*. Published master's thesis, Rochester Institute of Technology, Rochester, NY.

[8] Podhajny, R. M., Dr. (2004, April 1). Film wettability not so simple. *Paper, Film and Foil Coverters*. Retrieved March 15, 2007, from http://pffconline.com/mag/paper_film_wettability_not/#podhajnypic

[9] Uniting assembly and packaging. (2006, August 14). *Assembly Magazine*. Retrieved March 15, 2007, from BNP Media Web site: http://www.assemblymag.com/CDA/Archives/8ac1f3919fd0d010VgnVCM100000f932a8c0

[10] Version OLC3. (2007, November 19). *ESD guide*. Retrieved March 15, 2007, from http://www.static-sol.com/ESD_Guide/technical/definitions.htm

[11] Nylons (Polyamides) PA. (2003). *British Plastics Federation: Materials*. Retrieved March 15, 2007, from http://www.bpf.co.uk/bpfindustry/plastics_materials_Nylons_PA.cfm

[12] Nappi, J., Jr. (2004, May). A guide to ultra clean film packaging. *Clean Film Packaging*. Retrieved March 15, 2007, from Liberty Industry, Inc. Website: http://www.liberty-ind.com/clean_film_newsletter.html

[13] Selke, S. E., Culter, J. D., & Hernandez, R. J. (2004). *Plastics packaging* (2nd ed.). Munich, Germany: Hanser.

[14] Chase, G. (n.d.). Ohms per square what! *ESD Journal*. Retrieved February 23, 2007, from http://www.esdjournal.com/techpapr/ohms.htm

[15] Aisenbrey, T. (2002). *U.S. Patent No. 6,870,516*. Washington, DC: U.S. Patent and Trademark Office.

[16] DuPont Liquid Packaging Systems. (2006). *DuPont liquid packaging systems: High performance films—Dartek nylon 6,6 films*. Retrieved September/2006, from http://talasonline.com/photos/film/dartek_info.pdf

[17] NUANCE. (2006). *What is FT-IR?* Retrieved March 15, 2007, from http://www.nuance.northwestern.edu/KeckII/ftir1.asp

[18] *Surface tension*. (n.d.). [Brochure]. Cleveland, OH: Chemical Fabrics & Film Association.

[19] Williams, S. (2006, October 20). *Personal Communication*. Rochester, New York.

[20] RK Print Coat Instruments Ltd. (n.d.). *K printing proofer* [Pamphlet]. Retrieved September/October 2006, from http://www.rkprint.com/pdfs/printingproofer.pdf#search=%22RK%20printing%20proofer%22

[21] Metallic conductive inks. (2004, October 4). *Printed Electronics Review.* Retrieved September/October, 2006, from IDTechEx Web site: http://www.idtechex.com/printelecreview/en/articles/00000086.asp

[22] Harrop, P. (2006, February 28). Printing the Electronic Future. In *Printed Electronics World.* Retrieved September/October, 2006, from IDTechEx Web site: http://www.idtechex.com/printedelectronicsworld/articles/printing_the_electronic_future_00000449.asp

Prediction of Overprint Spectra Using Trapping Models: A Feasibility Study

J A Stephen Viggiano and Sri Hemanth Prakhya
Rochester Institute of Technology, School of Print Media
69 Lomb Memorial Drive, Rochester, NY 14623 (USA)
E-mail: jasv@acolyte-color.com; sreehemanth@gmail.com

Abstract

Overprints of two or more inks are used in models for prediction of color in halftone hardcopy and define several of the key boundaries in the color gamut of a system. The number of these overprints grows exponentially with the number of inks, making their measurement unwieldy for more than a few inks. It is desirable to have a method for predicting the color of overprints from measurements of the solid inks.

This paper explores the use of trapping models for overprint prediction. Two of the models, Hamilton's and Viggiano's simplification of Hamilton's model, produced accuracy levels which the researchers believe sufficient for previewing in graphic design software (ΔE^*_{ab} less than 4).

Introduction

In his seminal 1935 dissertation at Darmstadt, Neugebauer[1] pointed out that process color printing uses both additive and subtractive color mixing. The additive color mixing is spatially partite, pointillist (see, for example, *Un dimanche après-midi à l'Ile de la Grande Jatte* by Seurat), mixing of small areas of a discrete number of different colors. Each of these different colors, or end members, is a combination of the substrate and zero or more of the inks. The subtractive color mixing was the production of these endmembers by overprinting one ink atop another. These endmembers are now termed "Neugebauer Primaries" in Neugebauer's honor, and have several significant properties. First, they define, to a first order approximation, the gamut of the system to which they pertain. Secondly, even for non-linear models, which account for the Yule-Nielsen effect[2], they are the main parameters of models for printed color.

For three inks, there are eight Neugebauer primaries:

- Paper
- Cyan
- Magenta
- Yellow
- Red
- Green
- Blue
- Three-color overprint

There is one Neugebauer primary which contains zero inks; three which contain one ink; three which contain two inks; and one which contains all three inks. The sequence 1, 3, 3, 1 are the binomial coefficients for order three, and sum to eight.

For four inks, there will be sixteen Neugebauer primaries. Again, only one will contain none of the inks. Four of the primaries contain one of the inks; there will be six two-ink overprints and four three-ink overprints; only one primary will contain all four inks. The sequence 1, 4, 6, 4, 1 are the binomial coefficients for order four, and they sum to 16.

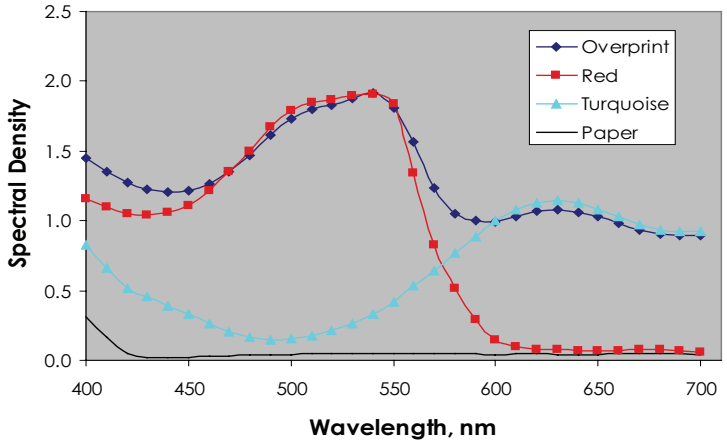

Figure 1. The density spectrum of an overprint is shown, together with the density spectra of the components which make it up: the first-down ink (red), the second-down ink (turquoise), and the unprinted paper.

Inks	Primaries	Fraction which are Multi-Ink
3	8	50.00%
4	16	68.75%
5	32	81.25%
6	64	89.06%
8	256	96.48%
10	1024	98.93%
12	4096	99.68%

Table 1. This table shows the exponential relationship between number of inks and number of Neugebauer primaries, as well as how the fraction of these primaries which contain two or more inks approaches 100 percent as the number of inks increases.

In general, for N inks, there will be 2^N Neugebauer primaries. This is a manageable number for small N, but, by definition, grows literally exponentially with the number of inks, as shown in Table 1. The fraction of the Neugebauer primaries which are overprints is nearly 90% for six inks, and is nearly 99% of them for ten inks. Further, total ink limit restrictions, both in standard lithographic printing (e.g., SNAP, GRACoL, SWOP) and for digital processes such as ink jet (where flooding of the paper is a concern when more than two solids are overprinted) may make it intractable to actually realize many of the Neugebauer primaries consisting of an overprint of two or more inks.

An application and initial motivation

Consider a problem faced by people using graphic design software, and printing with two or more spot colors, or one or more spot colors together with process inks. They may wish to use combinations of two or more spot colors, or one or more spot colors together with one or more process colors, to obtain a larger palette of colors without additional printing expense.

The overprint attributes available in graphic design software such as Adobe® Illustrator® do simulate overprints of spot colors (or a spot color and process color) through their "Overprint Preview" option. Thus, the desire of design professionals to create and use overprints in this manner has been acknowledged by publishers of such software. However, the researchers have observed that the on-screen appearance of these overprints is rarely a good match to the final printed result. It would help graphic design professionals to have accurate depiction on the monitor, as well as on inkjet proofs, of the colors produced by overprints involving one or more spot color inks.

Certainly, one could print samples of the inks, individually and overprinted, measure them, and produce an ICC named-color profile, for example, but this is impractical to do. There are over half a million combinations of two-ink overprints of Pantone® colors, neglecting print sequence. The approach investigated in this paper may be used to improve the accuracy of overprint predictions without the burden of producing, measuring, and compiling into a number of named colors into a massive profile.

An approach to estimating overprints

It is the researchers view that the spectrum of an overprint may be estimated from the spectra of the substrate and the two inks, which comprise it. Three ink overprints may then be estimated by treating the underlying two-ink overprint as the firstdown ink, and proceeding as if it is actually a two-ink overprint. This may be extended to as many inks as necessary. The models, which may be applied to these data to produce the estimated overprint spectra, are formulae for ink trapping, re-arranged to put overprint density on one side and everything else on the other. The justification for this is the notion that trapping values are intended to encapsulate the relationship between the densities of the substrate, the two inks, and the overprint.

In this paper, this process begins by examining the feasibility of overprint prediction for two inks. Future work may include three, four, or more inks.

Nomenclature: trapping formulae vis-a-vis trapping models

In this paper, reference is made to both trapping formulae and trapping models. The term "trapping formula" is used to refer to an equation which computes a number which characterizes the ratio of the "amount" (as quantified according to some criterion) of some ink when printed atop another ink to the amount of that same ink when printed atop previously unprinted substrate. The goal of a trapping formula is a number.

On the other hand, the term "trapping model" is used to refer to the assumptions, explicit or implicit, upon which a trapping formula is based. Thus, a trapping model may be thought of as the abstract, theoretical basis upon which a trapping formula is based. As a theoretical entity, a trapping model may be used to do things other than simply compute a trapping value, such as predict overprint spectra.

Trapping Formulae

At the time most of them were introduced, it was customary to report reflection densities relative to the unprinted paper. Since this is contrary to current standardized practice[5], the researchers have algebraically adjusted the formulae for absolute densities as required.

The Preucil Trapping Formula

Preucil's formula for trapping[6] uses densities as surrogates for ink layer thicknesses. The densities are measured through the complementary filter for the last-down ink, which tends to yield the greatest sensitivity to small changes in the thickness of the last-down ink.

$$T_p = \frac{(D_{12} - D_p) - (D_1 - D_p)}{D_2 - D_p} = \frac{D_{12} - D_1}{D_2 - D_p}$$

Equation 1. Preucil's formula, after accounting for non-zeroed-on-paper densities, where D_1 is the density of the first-down ink; D_2 is the density of the second-down ink; D_{12} is the density of the overprint; D_p is the density of the unprinted substrate; and T_P is Preucil's trap value.

As a decimal fraction, trapping is often expressed as a percentage. When using spreadsheet software to analyze data, one may use the formatting capabilities of the software to do this, rather than multiplying by 100%.

Typical values for Preucil trap tend to be between 70 and 95 percent for wet-on-wet printing with properly a tacked ink sequence.

Childers's Formula

Warren Childers, arguing that it was more valid to divide reflectances than densities, provided yet another formula[7].

$$T_c = 10^{-[(D_1 - D_p) + (D_2 - D_p) - (D_{12} - D_p)]} = 10^{D_{12} - D_1 - D_2 + D_p}$$

Equation 2. Childers' formula, taking into account the density of the substrate, where T_c is the Childers' trapping value.

Brunner Trap Formula

Brunner trap for properly tacked ink sequences are typically between 0.98 and 1.00. This narrow range has led to this formula being characterized as being insensitive to small changes in ink layer thickness under practical conditions[9].

$$T_b = \frac{1 - 10^{-(D_{12} - D_p)}}{1 - 10^{-(D_1 + D_2 - 2D_p)}} = \frac{1 - 10^{D_p - D_{12}}}{1 - 10^{2D_p - D_1 - D_2}}$$

Equation 3. System Brunner's proposed alternative formula to Preucil's[8], where T_b is the Brunner trap value.

Hamilton's Formula

John Hamilton of Kodak applied the Tollenaar-Ernst model[10] to permit a more accurate conversion from density to ink layer thickness, accounting for the phenomenon of subadditivity of densities[11], which results from the translucency of the last-printed ink. The base of the logarithms is arbitrary, as long as the same base is used for all four.

$$T_h = \frac{\log(D_\infty - D_{12}) - \log(D_\infty - D_1)}{\log(D_\infty - D_2) - \log(D_\infty - D_p)}$$

Equation 4. Hamilton's formula, after slight re-arrangement and accounting for non-zeroed-on-paper densities, where T_h is Hamilton's trap value.

The form of equation 4 bears some resemblance to the Preucil formula in equation 1. In both cases, trap is computed as the quotient of two binomials. In both equations, the numerator is the difference of some function of the overprint density and of the first-down ink; both denominators are the difference of some function of the density of the second-down ink and of the unprinted substrate. Similarly the function, which is applied, is assumed to transform density into something proportional to density; for the Preucil formula this is density itself, while for the Hamilton formula this function is a bit more complicated.

Linearized Hamilton formula (Viggiano's simplification)

$$T_v = \frac{D_{12} - D_1}{D_2 - D_p} \cdot \frac{D_\infty - D_p}{D_\infty - D_1}$$

Equation 5. Hamilton's formula simplified by linearizing it.

This formula may be interpreted as follows: The first fraction is the Preucil trapping formula. The second fraction is a linearized correction for subadditivity under the semi-logistic Tollenaar-Ernst model. The numerator of this second fraction is the total amount of density the second-down ink has to add above that of the paper; its denominator is the density the second-down ink may add above that of the first-down ink.

Ritz's formula

Professor Axel Ritz of the Hochschule der Medien/Stuttgart posed a recent suggestion, also based on Murray-Davies, like Brunner's, but arranged a bit differently[9]

$$T_r = \frac{1 - 10^{-(D_{12} - D_1)}}{1 - 10^{-(D_2 - D_p)}} = \frac{1 - 10^{D_1 - D_{12}}}{1 - 10^{D_p - D_2}}$$

Equation 6. T_r is the Ritz trap value.

Ritz points out that this formula is more sensitive to small changes in ink layer thickness. Again, note that the numerator involves differences between the densities of the overprint and the first-down ink (here, negated and in an exponential), while the denominator involves the difference between the densities of the second-down ink and the unprinted paper (again, negated and in an exponential).

Ritz offered the following justification for this model: Microphotographs of overprints revealed mottling in the second-down ink, producing a very fine halftone structure. This is consistent with the observations of Stollnitz[12] who integrated similar spatial features into a modification of the Neugebauer equations. (Stollnitz's work was published a year or two later than Ritz's, and was probably conducted independently.)

Models for Overprint Spectra Based on Trapping Models

In this section, the trapping formulae presented in the previous section will be re-arranged to provide the density spectrum of the overprint as functions of the spectra of the first- and second-down inks and substrate, together with a small number of parameters.

Overprint prediction based on Preucil's model

$$D_{12} = D_1 + T_p(D_2 - D_p)$$

Equation 7. Re-arrange of Equation 1 to obtain a prediction of overprint density.

$$D_{12,\lambda} = D_{1,\lambda} + T_p(D_{2,\lambda} - D_{p,\lambda})$$

Equation 8. This may be applied on a wavelength-by-wavelength basis to the density spectra of the substrate and the two single-ink solids to predict the density spectrum of their overprint

The researchers do not consider the Preucil trap value to vary with wavelength here, but rather assume it remains constant throughout the spectrum. (Indeed, the accuracy with which overprint spectra are reconstructed using non-spectral values of T_p may be regarded as a measure of both the robustness of the Preucil model, and the extent to which practical conditions satisfy the assumptions made in its derivation).

$$R_\lambda = 10^{-D_\lambda}$$

Equation 9. The density spectrum may be converted into a reflectance spectrum using the familiar relationship.

From this, the XYZ tristimulus values, CIELAB coordinates, etc., may be computed.

Brunner model

$$D_{12,\lambda} = D_{p,\lambda} - \log\left[1 - T_b\left(1 - 10^{2D_{p,\lambda} - D_{1,\lambda} - D_{2,\lambda}}\right)\right]$$

Equation 10. Brunner's trap formula may be inverted to provide overprint density as a function of the constituent densities and the Brunner trap value spectrally.

Again, we opt to use the same trap value throughout the spectrum.

Childers model

$$D_{12,\lambda} = D_{1,\lambda} + D_{2,\lambda} - D_{p,\lambda} + \log T_c$$

Equation 11. Solving Equation 2 for the overprint density, and writing all densities as spectra yields the equation above.

Hamilton model

$$D_{12,\lambda} = D_{\infty,\lambda} - (D_{\infty,\lambda} - D_{1,\lambda})\left[\frac{D_{\infty,\lambda} - D_{2,\lambda}}{D_{\infty,\lambda} - D_{p,\lambda}}\right]^{T_h}$$

Equation 12. Although Hamilton's trap formula appears the most complicated, it yields an overprint prediction model which is no more complicated than Brunner's.

The saturation density of the second-down ink, D_∞, usually varies throughout the spectrum, so it is written as a function of wavelength. There are not enough degrees of freedom available to fit both the parameter T_h and one value of D_∞ for each wavelength, so some constraints are necessary.

$$D_{\infty,\lambda} \approx \beta_0 + \beta_1 D_{2,\lambda}$$

Equation 13. Experience suggests that the saturation density spectrum may be approximated by the above formulae.

$$D_{12,\lambda} = \beta_0 + \beta_1 D_{2,\lambda} - (\beta_0 + \beta_1 D_{2,\lambda} - D_{1,\lambda})\left[\frac{\beta_0 + (\beta_1 - 1)D_{2,\lambda}}{\beta_0 + \beta_1 D_{2,\lambda} - D_{p,\lambda}}\right]^{T_h}$$

Equation 14. Substituting Equation 13 into Equation 12 yields the above equation.

Viggiano's simplification of Hamilton

$$D_{12,\lambda} = D_{1,\lambda} + T_v \frac{D_{\infty,\lambda} - D_{1,\lambda}}{D_{\infty,\lambda} - D_{p,\lambda}} (D_{2,\lambda} - D_{p,\lambda})$$

Equation 15. The overprint spectrum predicted by Viggiano's simplification of Hamilton's formula.

$$D_{12,\lambda} = D_{1,\lambda} + T_v \frac{\beta_0 + \beta_1 D_{2,\lambda} - D_{1,\lambda}}{\beta_0 + \beta_1 D_{2,\lambda} - D_{p,\lambda}} (D_{2,\lambda} - D_{p,\lambda})$$

Equation 16. Again, in many instances it may be necessary to constrain the D_∞ spectrum, substituting Equation 13 into Equation 15.

Ritz's Model

$$D_{12,\lambda} = D_{1,\lambda} - \log\left[1 - T_r\left(1 - 10^{D_{p,\lambda} - D_{2,\lambda}}\right)\right]$$

Equation 17. Re-arranging Equation 6 yields the formula for the overprint spectrum.

Experimental Approach and Methodology

Overprinted samples, together with the single-ink solids, were printed using lithography. Two combinations of inks were used: red and turquoise, and green and pink. The red and turquoise inks were printed in both sequences: red over turquoise, and turquoise over red. Because the printing was performed wet-on-wet, only one sequence was expected to trap well, because of tack sequence. The same procedure was repeated for the pink and green inks. The prints were then allowed to dry and were measured using an X-Rite® model 530 spectrophotometer.

$$D_\lambda = -\log(R_\lambda)$$

Equation 18. The measurements were imported into Microsoft Excel®, and converted to density spectra using this formula.

The pertinent spectra (first- and second-down solids, overprint, and unprinted substrate) were copied into separate worksheets to facilitate analysis.

Within each Excel® worksheet, six spectra were computed for the overprint, one according to each model. For the Hamilton and Viggiano models, the researchers used $\beta_0 = 1.5$ and $\beta_1 = 0.6$, which is believed to work reasonably well for normal ink layer thicknesses and for densities below 2.5. Each model thus had one parameter, the trapping value according to that model; these parameters were estimated by minimizing the CIELAB total color difference, ΔE^*_{ab}, between the actual overprint density spectrum and the overprint spectrum predicted by each model. Each model was given the benefit of the doubt regarding the specific trapping value; the researchers simply used the value which worked best for each model for each overprint. This is known as "entertaining the model," and is a standard practice in the scientific method. (13, at p 98, for example).

Overprint				
Model	R over T	T over R*	G over P*	P over G
Preucil	0.9784	0.5628	0.4986	0.8365
Childers	0.7948	0.8958	0.8785	0.8430
Brunner	0.9924	0.9366	0.9301	0.9471
Hamilton	0.9160	0.4744	0.5967	0.8626
Viggiano	0.9390	0.6064	0.6424	0.9010
Ritz	0.9977	0.9105	0.6750	0.9542

Table 2. This table shows the trapping values, optimized for each model/overprint combination. The overprints with a reverse tack sequence (higher tack ink printed over a lower tack ink) are indicated with an asterisk.

The predicted overprint density spectra were converted into reflectance spectra using Equation 9, then integrated using the ASTM E-308/ISO weights for the 2 degree observer/D50 illuminant to yield CIE XYZ tristimulus values. These were converted into CIELAB coordinates in accordance with ASTM/ISO procedures, and the CIELAB color difference, ΔE^*_{ab}, was computed for each prediction. This served as the figure of merit for the models under those particular conditions. Lower CIELAB color differences imply closer agreement between measured and predicted overprint spectra.

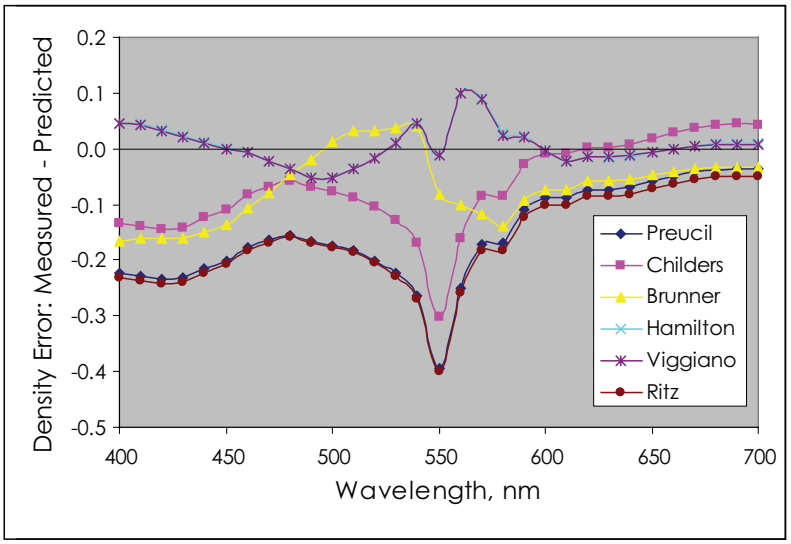

Figure 2. The errors of the six models tested in this investigation for the overprint plotted in Figure 1 (turquoise over red). (The errors for the Hamilton model are obscured by those of the Viggiano model because both models produced virtually identical predictions.)

Results

The optimized trapping values for each overprint/model combination appear in Table 2. As expected, the trapping values tend to be lower for the overprints with an incorrect tack sequence. Figure 2 also shows the spectral errors for one of the overprints with the correct tack sequence (turquoise over red). Because the predictions of the Hamilton and Viggiano models were nearly

identical, the error spectra for these two models are virtually indistinguishable, with one hiding most of the other. The CIELAB total color differences between the colors of the measured overprints and their predictions appear in Table 3.

The average error produced by each model is also presented in this table. The data in this table are summarized graphically in Figure 3. The ends of the error bars in this chart correspond to the smallest and largest CIELAB total color difference among the four predictions made by the corresponding model.

An Analysis of Variance (ANOVA) was performed on the ΔE^*_{ab} results; this is summarized in Table 4. The researchers tested the null hypothesis that the population mean ΔE^*_{ab}s produced by the different models were equal against the alternative that at least one population mean was different. the null hypothesis was rejected at the 0.05 significance level, and the researchers were able to conclude that at least one population mean was different from the others. This implies that not all of the trapping models predicted with equal accuracy.

	Overprint				
Model	T over R	R over T*	G over P*	P over G	Average
Preucil	5.22	1.69	2.11	7.84	4.21
Childers	3.80	23.84	11.67	8.33	11.91
Brunner	4.12	14.26	7.36	4.96	7.68
Hamilton	1.67	1.66	0.62	3.53	1.87
Viggiano	1.65	1.48	1.05	3.80	1.99
Ritz	5.29	8.56	2.53	8.67	6.26

Table 3. The performance of each model summarized by the CIELAB Total Color Difference, ΔE^*_{ab}, between the measured overprint and the predicted CIELAB coordinates based on the different models. Lower color differences mean more accurate predictions. The overprints printed with an incorrect tack sequence are flagged with an asterisk.

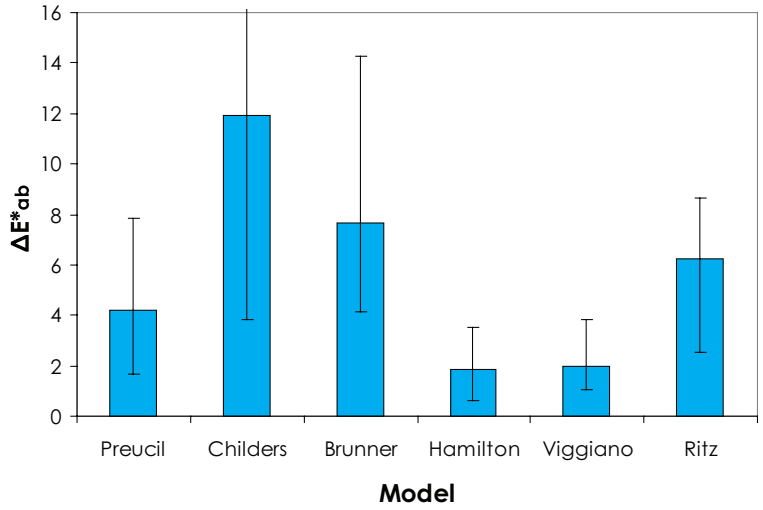

Figure 3. Results for four overprints, quantified by the CIELAB total color difference, ΔE^*_{ab}, between the measured overprint and the predicted CIELAB coordinates based on the different models. Lower color differences mean more accurate predictions. The lower and upper ends of the error bars correspond to the smallest and largest prediction errors for each model (the upper error bar for the Childers model is off scale at 23.8), respectively.

Source	SS	df	MS	F
Total (corrected)	637.73	23		
Models	293.56	5	58.71	3.07
Residual	344.17	18	19.12	

Table 4. The Analysis of Variance summary table for the null hypothesis of no difference among the models in average ΔE^*_{ab} against the alternative that at least one population mean ΔE^*_{ab} is different from the others. The p-value is 0.035, indicating at least one statistically significant difference among the population means.

Conclusions

The Hamilton and Viggiano models performed the best in this investigation. An explanation for this is that of the models tested, only these two take into account the subadditivity phenomenon caused by scatter in the top-down ink. These models also performed similarly to each other. This may be attributed to one (the Viggiano model) being a linearized simplification of the other (the Hamilton model).

The average CIELAB total color difference for both these models is under 2, and the largest is under 4 in both cases. This performance should be satisfactory for most practical purposes.

In fairness to the models which did not predict overprints as accurately (and to those who derived them), the researchers point out that this was not the goal of any of the trapping models. Nevertheless, their fitness is discussed for this purpose in the paragraphs below, with the understanding that such discussion is not intended to cast aspersions on the fitness of these models for their intended purpose.

Two other models that tended to perform similarly to each other were the Preucil and Ritz models, especially for the properly tacked print sequences (turquoise over red and pink over green); the single case for which they showed significant disagreement was one of the overprints with the reverse tack sequence (red over turquoise). The Preucil model computes trap as the ratio of two density differences, while the Ritz model computes trap as the ratio of the two absorbances (absorbance here being the complement of reflectance) corresponding to the same two density differences.

Surprising was the difference between the Ritz and Brunner formulae, which appeared quite similar mathematically. Both are ratios of absorbances, but the absorbances are computed slightly differently. Between these two, the Ritz model performed slightly better, yielding both lower prediction errors, and less erratic predictions than the Brunner model.

For Future Work

The researchers believe that the feasibility of overprint prediction has been established through this report. It would be fruitful to investigate this in greater depth, using more overprints, perhaps using other printing processes, like flexography and gravure.

The sensitivity of the prediction to the trapping value should be investigated. In practice, the techniques discussed in this paper will be applied without the benefit of optimized trapping values. Before these methods can be applied, one should know the influence an imprecise estimate of the trap parameter has on accuracy. If a generic value such as, say, 0.90 for the Viggiano model is used, will the results be any less accurate than, for example, those currently displayed in the Overprint Preview in Adobe® Creative Suite®?

If the robustness of the technique developed here is demonstrated, the technique may be extended to overprints of more than one ink. This will be helpful in model-based characterization.

Acknowledgements

The authors wish to thank the Printing Applications Lab at RIT for performing the special press run, and their advisers, Professor Dr. Franziska Frey and Professor Robert Chung, for their encouragement.

References

[1] Neugebaur, H. E. J. (1937, April). Die theoretischen Grundlagen des Mehrfarbenbuchdrucks. *Zeitschrift für wissenschaftliche Photographie Photophysik und Photochemie, 36*(4), 73-89.

[2] Yule, J. A. C., & Neilsen, W. J. (1951). The penetration of light into paper and its effect on halftone reproduction. *TAGA Proceedings*, 65-76.

[3] Hamilton, J. F. (1985). Ink trap: the moving target. *TAGA Proceedings*, 397-403.

[4] Field, G. G. (1985). Ink trap measurement. *TAGA Proceedings*, 382-396.

[5] Committee for Graphic Arts Technologies Standards. (2006). *Graphic technology – Graphic arts densitometry measurements – Terminology, equations, image elements and procedures*.

[6] Preueil, F. (1952). Color hue and ink transfer-their relation to perfect reproduction. *TAGA Proceedings*, 102-110.

[7] Childers, W. (1980, December). Expert shows math path to avoid ink trap. *Graphic Arts Monthly, 52*(12), 63-64.

[8] E I du Pont de Nemours and Co, Inc. (1984). *Chromalin Offset Com Guides/system Brunner* [Brochure].

[9] Ritz, A. (1996, September/). A halftone treatment for obtaining multi-colour ink film trapping values. *Professional Printer, 40*(5), 11-17.

[10] Tollenaar, D., & Ernst, P. A. H. (1961). Optical density and ink layer thickness. *Problems in high speed printing: Proceedings of the Sixth International Conference of Printing Research Institutes*, 214-234.

[11] Hamilton, J. F. (1986). A new ink-trap formula for newsprint. *TAGA Proceedings*, 158-165.

[12] Stollnitz, E. J. (1998). *Reproducing Color Images with Custom Inks*. Unpublished doctoral dissertation, University of Washington, Seattle, WA.

[13] Box, G. E. P., & Jenkins, G. M. (1968). Some recent advances in forecasting and control, part I. *Applied Statistics, 17*(2), 91-109.

The Influence of Coating on the Paper and Printing Properties of LWC Paper

Yu-Ju Wu
Center for Ink and Printability Research
Department of Paper Engineering, Chemical Engineering and Imaging
Western Michigan University, Kalamazoo, MI, U.S.A.

Abstract

The main objective of this study was to evaluate the influence of coating compositions, namely different latex polymers, on paper properties and the impact of the paper properties on printing properties. Seven kinds of latex polymers were used in coating formulation, and coated in the same condition. The final paper properties such as roughness, formation, pore size, porosity, air permeability, brightness, opacity, and paper gloss were tested. The coated papers were then printed on a Cerutti Model 118 rotogravure web press. Printed paper samples were collected and printing properties including dynamic penetration, print gloss, and print mottle were evaluated and compared. The results show that sample 1 yields a smoother paper surface, smaller porosity-related characteristic readings and higher print gloss, but poor paper sheet uniformity. Color reproduction capability (color gamut volume) was similar for all coating formulations.

INTRODUCTION

Light weight coated paper (LWC), one of the most widely used gravure publication grades, has a coat applied on the base paper sheet to mask the roughness and void spaces, providing a smooth surface that gives a detailed, uniform, defect free image when printed. The coating layer covers the fibers and voids to improve paper properties such as brightness, gloss, smoothness and uniformity. The coating layer also improves the print quality by holding the ink on the surface of the paper and for creating a detailed uniform printed image (Larsson & Engstrom, 2004).

Paper coating is a composite material consisting of pigment, binder and performance enhancing additives along with air-filled voids. The pigment particles are bound together by binder in a porous network. Their arrangement on the base paper makes up the coating structure. Changes in pigment composition, type and amount of binder and additives produce different coating layer microstructures. The coating structure in turns affects ink setting speed and uniformity, which are important in achieving high print quality (Vincent, 1996; Laudone, Matthews & Gane, 2006; Kentta, Pohler & Juvonen, 2006; Pohler, Juvonen & Sneck; 2006; Triantafillopoulos & Lee; 1997). Styrene butadiene latexes are used in publication gravure coatings in the U.S., while styrene acrylates have been used in Europe. Acrlyonitrile added to SB provides solvent resistance.

Latex polymers, most widely used as pigment binders for various types of coated papers, are used for the purpose of binding the pigment particles to each other, binding the coating components to the base stock, providing the required strength for the coated paper to pass through the printing and converting operations, and yielding improved sheet gloss, ink gloss and printability (Bergh, 1997; Laudone, et al., 2005). The mechanical properties of the coating layer depend on not only the cohesion of the latex bridges formed between the pigment particles, but also the adhesion between the latex and pigment particles and void structure of the coating layer. Indeed, pore structure is mainly affected by pigments, but the location of latex in the structure may influence the final paper properties. Furthermore, the type of latex used in the coating formulation will affect the strength and absorbency characteristics of the coated paper. These coating characteristics determine the rate of ink penetration and amount of ink transferred to the paper (Kentta, Pohler & Juvonen, 2006; Ratto, 2004; Forbes, Triantafillopoulos & Lallemant, 1998).

The uniformity of ink absorbency and color density are greatly influenced by the paper coating characteristics. The most important surface properties of paper include roughness, formation, porosity and air permeability. Roughness and formation are

considered as external surface properties, while pore size, porosity and air permeability are categorized as internal surface properties. Roughness affects print gloss and color, as well as print contrast. Formation is an indicator of how uniformly the fibers and fillers are distributed in the sheet. Formation plays an important role as most of the paper properties depend on it. A poorly formed sheet will have more weak and thin or thick spots. Paper formation will affect the printing characteristics of the paper (Wilson, 1997; Biermann, 1996; Peel, 1999). The porosity of a paper sheet is the ratio of pore volume to total volume and it greatly affects properties such as hardness, compressibility, resiliency, and the ability to absorb inks. Air permeability is defined as the property of a paper that allows air to flow through it under a pressure difference across the sheet. The air permeability is also an indicator that shows how printing inks will penetrate and spread (Wilson, 1997; Scott & Abbott, 1995). The coating characteristics also affect paper optical properties. The optical properties of a paper influence the visual quality of the printed image and contribute to its appearance and appeal. The best color reproduction will occur with papers that are bright with uniform spectral reflection, smooth, glossy, and neutral shade. The key optical properties include brightness, opacity, and paper gloss. The higher the brightness, the higher the contrast between the paper and printed image is (Lee, Joyce & Fleming, 2005). Opacity is a measure of a paper's ability to obstruct the passage of light. Too much show-through of printed images from the back side of the sheet will reduce print contrast and interfere with the visual appearance of the image. Paper gloss is the attribute of paper surface that makes the images look shiny or lustrous. The gloss of a paper affects the color of a print because it affects the way light is reflected through the ink. In order to maintain uniform color printing throughout a job, the variations in gloss must be monitored and kept to a minimum level. Glossy papers are usually associated with high surface smoothness and good printing quality. High quality printed images also come up with high gloss by increasing the gloss of printed ink films and enhances the brilliance and color intensity of printing (Wilson, 1997; Levlin & Soderhjelm, 2000; Thompson, 1998).

Experiments continue to be designed to provide the appropriate paper and ink interaction and produce high quality images to meet printing and paper manufacturing demands (Vincent, 1996; Laudone, et al., 2005). The main objective of this study was to evaluate latex effects on paper properties and then the impact of the paper properties on printing properties. Different types of latex polymers are considered in the coating formulations to evaluate their influence on final paper properties, ink transfer and print quality.

EXPERIMENTAL

Coating Formulations

Six styrene butadiene acrylonitrile (SBA) latexes were used in this study. Styrene-butadiene (SB) was used for the latex, too. Key characteristics of the latexes selected for this paper are listed in **Table 1**. Latex polymers were formulated into a pigment system consisted of 80 parts delaminated clay and 20 parts of No. 1 clay, using 6 parts latex based on pigment and 0.1 part disperser (Dispex N40) with RM 232 thickener. Each latex was evaluated as the sole binder in the coating formulation which was applied to base paper of 44.82 g/m^2 basis weight. Coating formulations are shown in **Table 2**.

Table 1: Key characteristics of latexes

Latex	Chemistry	Particle Size	Degree of carboxylation	Tg (°C)
Latex A	styrene butadiene (SB)	Large	Low	-28
Latex B	styrene butadiene acrylonitrile (SBA)	Large	Low	-2
Latex C	styrene butadiene acrylonitrile (SBA)	Large	Low	-25
Latex D	styrene butadiene acrylonitrile (SBA)	Medium	Low	10
Latex E	styrene butadiene acrylonitrile (SBA)	Medium	Low	-15
Latex F	styrene butadiene acrylonitrile (SBA)	Medium	Low	-6
Latex G	styrene butadiene acrylonitrile (SBA)	Medium-Large	Low	-6

Table 2: Coating formulations (added amount: parts per hundred, pph)

Sample ID		1	2	3	4	5	6	7
Pigment	Delaminated clay, Astraplate	80	80	80	80	80	80	80
	No. 1 clay, KCS	20	20	20	20	20	20	20
Latex polymer	Latex A	6						
	Latex B		6					
	Latex C			6				
	Latex D				6			
	Latex E					6		
	Latex F						6	
	Latex G							6
Thickener	RM 232	✓	✓	✓	✓	✓	✓	✓
Disperser	Dispex N40	0.1	0.1	0.1	0.1	0.1	0.1	0.1

Paper Properties Testing

The key properties evaluated included surface properties (roughness, formation, pore size, porosity, and air permeability) and optical properties (paper gloss, brightness, and opacity). The instruments used for paper properties measurement were summarized in **Table 3**. An Electronic Microgage Model 210-R (Emveco, Inc) with the spherical steel stylus having a radius of 0.001 inch was used for profilometer measurement. An Autopore IV 9500 mercury porosimeter, measuring the incremental increase of volume penetrated as the pressure rises, was employed for the porosity-related characteristics measurement such as of pore size, volume, and distribution of a paper. A Brightimeter MICRO S-5 was

employed to measure brightness %, complying with TAPPI standard T 562 (C illuminant with 45°/0° geometry). A BNL-2 opacimeter was employed to test opacity, using TAPPI standard T 425 (opacity = R_0 / $R_{0.89}$). Paper gloss at 75˚ was measured using a Novo-Gloss™ Glossmeter based on TAPPI standard T 480.

Table 3: Instruments used for paper properties measurement

Paper Properties	***Measuring Instrument***
Emveco Roughness [μm]	EMVECO stylus profilometer
Formation Index	M/K system formation tester
Pore Size [nm]	Mercury intrusion porosimetry
Porosity [%]	Mercury intrusion porosimetry
Air Permeability Coefficient [μm^2]	Parker Print-Surf (PPS) tester Using equation of K = 0.048838 * Q * X Q=PPS Porosity; X=thickness
Brightness [%]	Brightimeter MICRO S-5 (C/2°)
Opacity [%]	BNL-2 Opacimeter (TAPPI Standard)
Paper Gloss [%]	Novo-Gloss™ Glossmeter (at 75°)

Printing Procedure

The coated papers were printed on a rotogravure web press Model 118 from Cerutti Group (Italy), located at the Western Michigan University (WMU) Printing Pilot Plant. Commercial toluene-based coated yellow, magenta, cyan and black inks for rotogravure from Flint Group were used. The ink efflux time with Shell cup #2 was kept at 22 ± 0.5 seconds for yellow and magenta, 25 ± 0.5 seconds for cyan, and 20 ± 0.5 seconds for black ink, respectively. Printing was done at 600 ft/min with electrostatic assist (ESA) on. The target print densities were 1.00 for yellow, 1.35 for magenta, 1.35 for cyan, and 1.50 for black, which was achieved for the first printed substrate, and then the same printing condition was maintained during the printing process of the rest of the substrates.

Printing Properties Testing

Printed paper samples were collected and their printing properties were evaluated in terms of dynamic penetration test, print gloss, and print mottle (ink uniformity). The absorption characteristics of tested paper samples were measured using Emco Dynamic Penetration Measurement (DPM), which is equipped with DPM software version 3.31. The Emco DPM works by sending ultrasonic pulses through a fluid medium, where paper has been submerged, and based on how long the ultrasonic pulses would take to reach its respective receiver [19]. Paper gloss and print gloss at 60˚ was measured using a Novo-Gloss™ Glossmeter. The delta gloss values were then calculated from "print gloss – paper gloss." The color reproduction capability (color gamut) was evaluated in terms of gamut volume. **Table 4** lists the instruments/software used for printing properties/color reproduction capability measurement.

RESULTS AND DISCUSSION

This study evaluates the influence of seven different latex polymers on paper properties and then the impact of the paper properties on printing properties and color reproduction capability. The correlations between paper surface properties and printing properties/color reproduction capability were investigated.

Table 4: Instruments used for printing properties/color reproduction capability measurement

Printing Properties	***Measuring Instrument/Software***
Dynamic Penetration Test	Emco Dynamic Penetration Measurement (DPM) Measuring area: 10mm-diameter
Paper Gloss	Novo-Gloss™ Glossmeter (at 60°)
Print Gloss	Novo-Gloss™ Glossmeter (at 60°)
Verity Print Mottle	Verity IA Color Image Analysis software (equipped with a scanner)
Color Gamut (Gamut Volume)	Target: ECI 2002R Measuring Tool: X-Rite DTP70 Spectrophotometer Profiling Software: X-Rite MonacoPROFILER 4.8 Gamut Evaluation Software: CHROMiX ColorThink 3.0 Pro

Paper Properties

Table 5 summarized paper properties testing results. Roughness is one of the most important factors affecting print quality. A smoother surface can result in a good ink transfer, and vice versa (Wilson, 1997; Thompson, 1998). The average roughness readings for the tested samples are in the range of 1.3 to 1.6 micron (**Table 5**). At the same time, sample 1 has a smoother surface, while sample 4 has a rougher surface than the rest of the papers.

The porosity of a paper determines ink setting speed and uniformity. The highest percent porosity was found in the sample 2 with 65.0% (**Table 5**). Sample 6 has the lowest percent porosity at 56.5%. The average pore size readings for the tested samples are in the range of 180 to 240 nm. Sample 2 tends to have a larger pore size, while sample 1 has a smaller pore size. The pore size distribution of all tested paper samples is shown in **Figure 1**. All tested paper samples have peaks of pore sizes between 100 to 10,000 nm. The pore sizes over 10,000 nm (not shown) were not considered, since they originate from raw stock porosity and possible artifacts. Air permeability, a porosity-related characteristic, is the property of a paper that allows air to flow through it under a pressure difference across the thickness of the sheet. The permeability coefficient of each substrate was calculated from the Parker Print Surf porosity value and its thickness using the Pal equation:

$$K = 0.048838 * Q * X \quad (1)$$

where K is the permeability coefficient in μm^2, Q is the flow rate of PPS 500 kPa in ml/min and X is the sheet thickness in m (Pal, Joyce & Fleming, 2006).

Table 5: Paper properties measurement

Surface Properties								
Sample ID	Emveco roughness [μm]		Ave. pore size [nm]	Porosity [%]	Air permeability coefficient [μm^2]		Formation index	
	Mean	Std. Dev.			Mean	Std. Dev.	Mean	Std. Dev.
1	1.38	0.06	203.0	59.8	$10.6x10^{-6}$	$9.8x10^{-7}$	11.8	0.9
2	1.58	0.07	239.2	65.0	$21.3x10^{-6}$	$21.5x10^{-7}$	18.4	1.7
3	1.59	0.08	204.2	63.4	$22.8x10^{-6}$	$22.3x10^{-7}$	18.6	2.0
4	1.60	0.06	232.7	64.1	$24.9x10^{-6}$	$26.6x10^{-7}$	23.0	0.9
5	1.51	0.06	208.8	62.1	$19.3x10^{-6}$	$18.4x10^{-7}$	18.8	1.3
6	1.58	0.06	188.6	56.5	$23.4x10^{-6}$	$20.5x10^{-7}$	17.5	1.5
7	1.54	0.07	231.6	60.9	$21.6x10^{-6}$	$18.4x10^{-7}$	20.2	2.9

Optical Properties						
Sample ID	TAPPI Brightness [%]		TAPPI Opacity [%]		Paper gloss at 75° [%]	
	Mean	Std. Dev.	Mean	Std. Dev.	Mean	Std. Dev.
1	69.9	0.1	82.0	0.7	49.7	1.8
2	70.6	0.2	82.5	0.6	48.8	1.7
3	70.6	0.2	82.5	0.5	44.1	0.6
4	70.4	0.3	82.7	0.5	50.3	2.1
5	70.5	0.1	82.1	0.6	50.6	1.1
6	70.4	0.3	82.2	0.6	48.5	1.6
7	70.8	0.6	82.3	0.8	48.5	2.2

It shows that sample 1 has the lowest air permeability coefficient value of 10.6×10^{-6} μm^2 and smallest standard deviation value, while sample 4 has the highest air permeability coefficient value of 24.9×10^{-6} μm^2 and largest standard deviation value. In other words, less air flows through sample 1.

Formation is a measurement of uniformity of the paper (Wilson, 1997). A formation index is used to evaluate formation, which measures the relative uniformity of paper on the basis of localized variations in basis weight. The larger the formation index, the more uniform the sheet (Biermann, 1996). An M/K system formation tester was employed to obtain formation index values, which measure variations in light transmitted through the tested sheet as the light source scans across the sheet rapidly. **Table 5** shows that sample 4 is more uniform than other tested samples. As shown in **Table 5**, the average brightness readings for the tested paper samples are in the range of 69 to 71%. Sample 7 is slightly brighter than other tested samples. The higher the opacity, the better the hiding power is and less show through [12, 16]. The average opacity readings for the tested paper samples are in the range of 81 to 83%. Papermaking gloss is the attribute of paper surface that makes the images look shiny or lustrous. The paper gloss affects the color of a print because it affects the way light is reflected through the ink. Sample 5 has highest paper gloss of 50.6%, while sample 3 has lowest paper gloss of 44.1%.

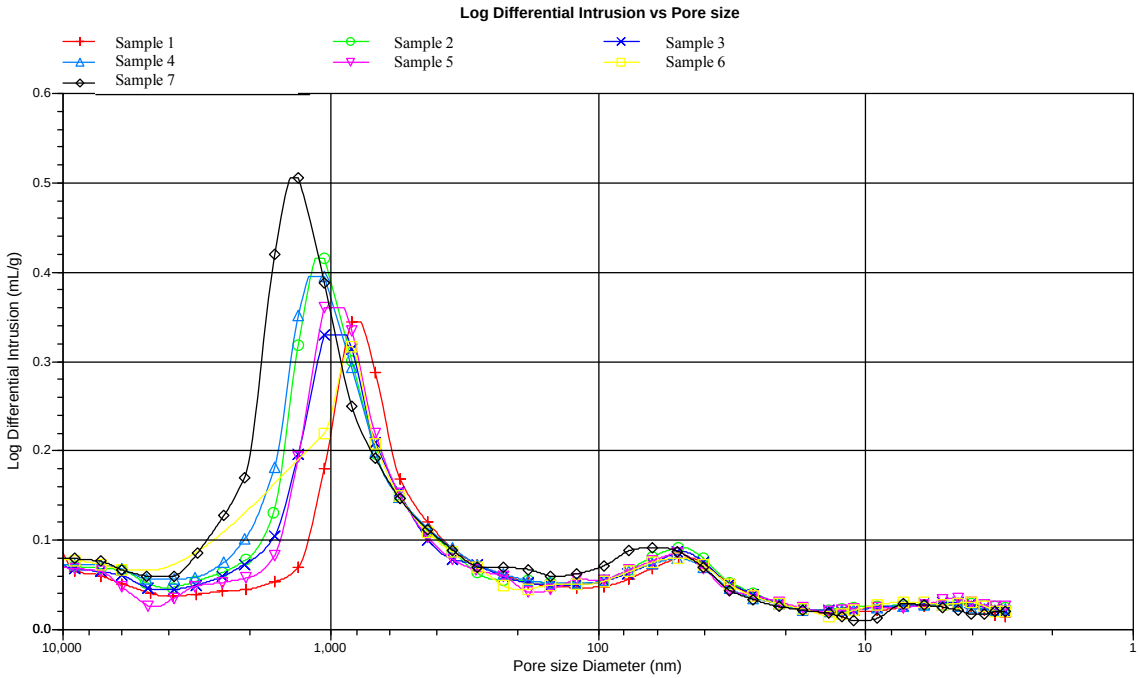

Figure 1: Pore size distribution from mercury porosimetry curves

Printing Properties

The Emco dynamic penetration test can be considered as an indicator to predict ink-paper interaction. In this study, paper samples were printed using toluene-based ink. Both deionized water (DI water) and toluene served as testing liquids at 23˚C. The dynamics of DI water/toluene and tested paper sample interactions are illustrated in **Figure 2**.

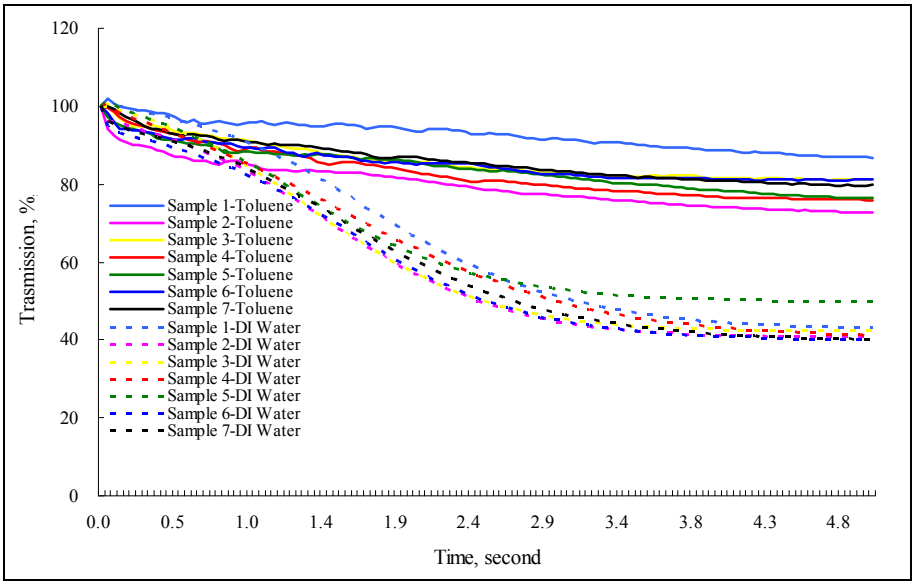

Figure 2: Water penetration characteristics of tested samples

There are obvious differences between a water ultrasound curve and a toluene ultrasound curve. It shows that all paper samples absorbed more DI water (dashed-line) than toluene (solid-line) after one second. In the case of treating with toluene fluid, the fastest penetration was found in sample 2 (magenta solid-line), while sample 1 (cyan solid-line) absorbs the least amount of toluene during the whole 5 seconds of measurement interval. It is interesting to note that toluene somehow swells the structure of sample 1 (cyan solid-line) between 0.5 to 3.0 seconds. Possible reason for this is that the interaction occurs between toluene and coating layer, resulting in impregnating the structure. In terms of DI water fluid, all tested paper samples absorbed water immediately (within 3.5 seconds) after they came into the contact with water and tend to have similar absorption curve. The slowest penetration was also found in the sample 1 (cyan dashed-line). Sample 1 has relatively low air permeability and smaller average pore size, which correlates with its slower fluid penetration rate.

The print gloss is obtained after the application of ink, usually in solid patches. It depends on the surface gloss of the paper and also on the degree of absorption of ink into the paper. Both the color appearance and its intensity will change along with ink penetration. Printed papers having high gloss can provide good color saturation, whereas printed papers with low gloss will have a dull unsaturated appearance. In most situations, papers required to carry multicolor printing need a high gloss to give intensity or color saturation (Thompson, 1998). The measurement of print gloss and delta gloss of tested papers is shown in **Table 6**. It displays that sample 1 yields higher print gloss and can achieve higher positive delta gloss due to less ink penetration into the paper sheet. Sample 4, on the other hand, has lower print gloss. Tested paper samples have higher print gloss in cyan and lower print gloss in yellow. A higher gloss contrast between printed and unprinted areas was found in cyan and black inks.

Table 6: Gloss measurement at 60° geometry

Sample No.		1	2	3	4	5	6	7
Paper gloss		23.9	17.5	16.7	16.6	18.1	17.6	16.4
Cyan	Print gloss	43.7	32.5	30.6	30.6	34.2	32.3	32.4
	Delta gloss	*19.8*	*15.0*	*13.9*	*14.0*	*16.1*	*14.7*	*16.0*
Magenta	Print gloss	35.1	28.9	26.6	23.8	27.3	26.8	26.1
	Delta gloss	*11.2*	*11.3*	*9.9*	*7.2*	*9.2*	*9.2*	*9.7*
Yellow	Print gloss	32.8	26.6	24.4	24.4	26.7	25.1	25.7
	Delta gloss	*8.8*	*9.1*	*7.7*	*7.7*	*8.6*	*7.5*	*9.3*
Black	Print gloss	41.4	30.3	29.2	28.1	31.7	29.8	29.2
	Delta gloss	*17.5*	*12.8*	*12.4*	*11.5*	*13.6*	*12.2*	*12.8*

A common printing defect of coated papers in multicolor printing is print mottle (irregular and unwanted variations in the printed tone). The distribution uniformity of the

coating components is one factor influencing coated printing paper mottle. If the coating surface receives a uniform ink film, uneven surface binder distribution may create differences in ink penetration, causing print mottle (Kentta, Pohler & Juvonen, 2006; Pohler, Juvonen & Sneck, 2006; Zang & Aspler, 1998). Scanned solid CMYK patches were evaluated with Verity IA Color Image Analysis software. The print mottle measurement algorithm is a derivative of the Verity IA stochastic frequency distribution analysis. It quantifies the degree of mottle present in printed specimens. The greater the print mottle number, the greater the variations in surface fiber (Rosenberger, 2006). **Table 7** shows the measurement of print mottle of tested paper samples. As shown in **Table 7**, sample 1 has lower print mottle numbers in cyan and black, while sample 4 has a lower print mottle number in magenta. All tested paper samples have smaller print mottle numbers in yellow, in other words, the print mottle in yellow is less obvious.

Table 7: Print mottle measurement

Sample ID	Cyan		Magenta		Yellow		Black	
	Mean	Std. Dev.	Mean	Std. Dev.	Mean	Std. Dev.	Mean	Std. Dev.
1	12.6	1.2	10.6	2.5	5.7	1.8	3.9	0.2
2	16.4	2.9	17.1	1.1	4.6	1.0	7.6	0.8
3	21.3	3.8	15.0	3.8	4.5	0.5	9.2	0.6
4	13.0	2.1	8.1	1.0	4.2	0.9	7.8	0.8
5	16.7	5.3	13.6	3.0	3.8	0.5	7.4	0.6
6	20.0	3.2	10.1	0.9	3.7	0.6	8.9	0.6
7	14.3	2.9	12.1	1.9	3.8	0.4	9.2	0.7

The color gamut is the range of colors that a particular combination of press, ink, and print media can achieve. The wider the color gamut, the more colors the press can reproduce. Therefore, color gamut can be treated as an indicator predicting color reproduction capability of a device (Chovancova-Lovell & Fleming, 2008). The color gamut comparisons for the tested paper samples are shown in **Figure 3** and **Table 8**. The color gamut volumes of tested paper samples are quite similar to each other. The gamut volume of a printer/substrate combination is the volume of the gamut figure in $L^*a^*b^*$ space. It can be interpreted as the number of independent colors that can be printed on the designated substrate within a ΔE tolerance of $\sqrt{3}$ (i.e. the diagonal of a unit cube). Recently, gamut volume with a given printing device has been proposed as a measure of the quality of paper and its coating (Chovancova, et al., 2005). The gamut volumes are in the range of 300,000 to 325,000. In other words, the types of latex used in this study didn't make big difference in the color reproduction.

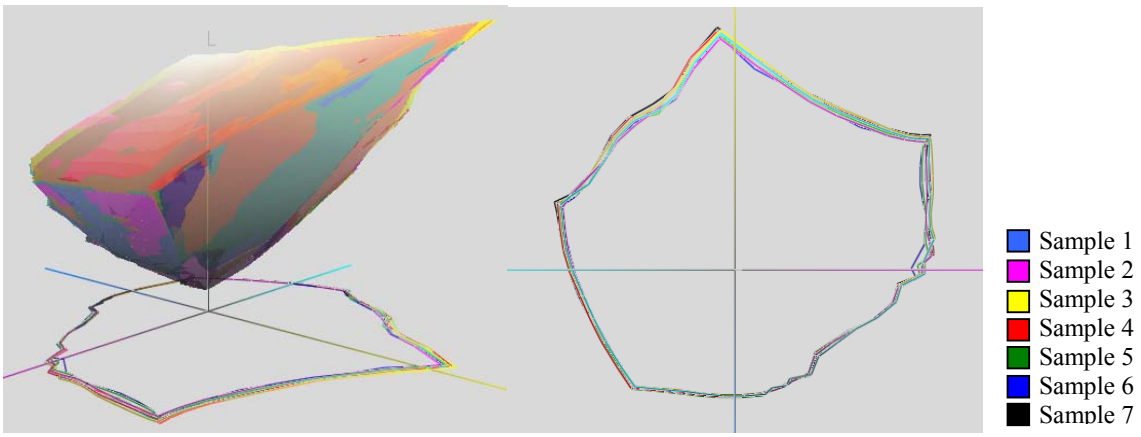

Figure 3: Color gamut comparison for the tested paper samples

Table 8: Gamut volumes comparison for the tested paper samples

Sample ID	Gamut Volume	
	Mean	Std. Dev.
1	316,000	3,000
2	322,000	3,000
3	315,000	4,000
4	313,000	4,000
5	311,000	4,000
6	313,000	3,000
7	306,000	4,000

Correlation Analysis for Surface Properties and Printing properties

The printability of a paper surface is influenced by surface properties, such as smoothness, the uniformity with which the surface accepts ink transfer from the printing plate, and the paper's absorption of the ink. This section investigates the correlations between paper surface properties and printing properties. Pearson's correlation coefficient was used to measure association between paper surface properties and printing properties. The significant level (α) was set at .05 for statistical tests. The correlation analysis results about the relationship between the paper surface properties and printing properties are exhibited in **Table 9**. It shows that the roughness of the tested paper samples significantly correlates with print gloss at the 0.05 level. With decreasing roughness, print gloss increases. It also found that there is a strong negative relationship between formation and print gloss. There is no significant correlation between formation and print mottle. The correlations between porosity-related characteristic and printing characteristics were not clear (p value > α = .05), with the exception of air permeability. There is a strong negative relationship between air permeability and print gloss. The air less flows through the paper sheet, the higher the print gloss is. The air permeability of the tested paper samples also significantly correlates with print mottle in yellow and black color.

Table 9: Pearson correlation between paper surface properties and printing properties

Printing properties		Roughness		Formation		Average pore size		Porosity		Air Permeability	
		Sig. 2-tailed	Pearson Correlation	Sig. 2-tailed	Pearson Correlation	Sig. 2-tailed	Pearson Correlation	Sig. 2-tailed	Pearson Correlation	Sig. 2-tailed	Pearson Correlation
Print gloss	C	**.000**	**-.976***	**.009**	**-.879***	.509	-.303	.451	-.343	**.002**	**-.935***
	M	**.009**	**-.880***	**.001**	**-.956***	.524	-.293	.575	-.259	**.002**	**-.938***
	Y	**.001**	**-.958***	**.010**	**-.873***	.672	-.197	.601	-.242	**.002**	**-.937***
	K	**.001**	**-.960***	**.005**	**-.905***	.452	-.342	.500	-.309	**.001**	**-.955***
Print mottle	C	.253	.500	.919	.048	.231	.452	.738	-.156	.517	.298
	M	.755	.146	.838	-.096	.630	.223	.289	.469	.847	-.090
	Y	.104	-.663	.074	-.710	.939	-.036	.778	.289	**.031**	**-.800***
	K	**.011**	**.869***	.065	.725	.806	.115	.880	.071	**.018**	**.838***

* Correlation is significant at the 0.05 level (2-tailed).

Figure 4 displays relations between roughness and printing properties. It shows that there is a strong correlation between roughness and print gloss, consistent with previous results (Xu, et al., 2005; Xu, 2006). Print gloss increased as roughness of paper decreased. The relationship between roughness and print mottle is not clear. As shown in **Figure 4**, the print mottle number slightly increased as roughness of paper increased for cyan and black, that is, the more uniform the paper, the less the print mottle in cyan and black color.

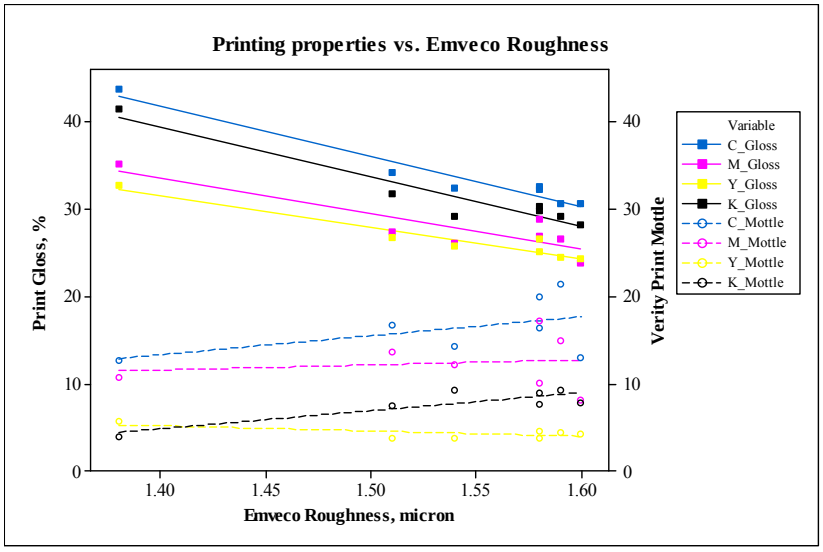

Figure 4: Relationship of Emveco roughness vs. printing properties

Figure 5 illustrates relations between formation and printing properties. It shows that a strong negative relationship was found between formation and print gloss. In other words, the more uniform the paper, the lower the print gloss can be obtained. This negative relationship needs further investigation, as it is counter intuitive. The relationship between formation and print mottle is not clear. **Figure 5** indicates that print mottle slightly increased as formation index of paper decreased for black, that is, the more uniform the paper, the less print mottle appeared in black color.

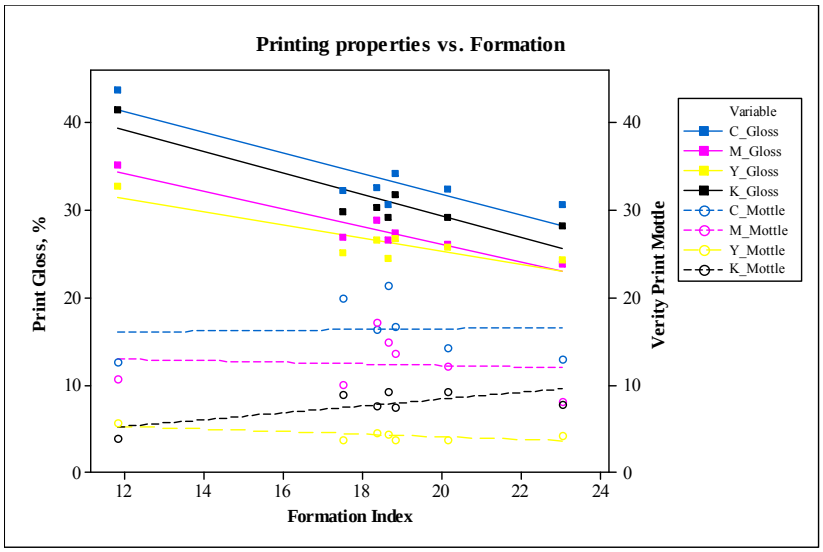

Figure 5: Relationship of formation vs. printing properties

Figure 6 to **Figure 8** exhibit relations between porosity-related characteristics and printing properties. There are no strong relationships between porosity-related characteristics and printing properties, except for air permeability. As shown in **Figure 6** and **Figure 7**, print gloss value slightly increased as average pore size and porosity value decreased, which means grooved structures and convergent pore geometries may decrease print gloss. According to **Figure 6**, **Figure 7**, and **Table 9**, print mottle slightly increased as average pore size and porosity value increased. In other words, grooved structures and convergent pore geometries may increase print mottle permanence. As shown in **Figure 8**, a significant relationship was found between air permeability and print gloss. The less the air flows through the paper sheet, the higher the print gloss is. This may be related to low air permeability values being observed in coatings with small pigment particle size, which also tend to generate high paper and ink gloss (Lee, Joyce & Fleming; 2005; Xu, et al., 2005; Chovancova, et al., 2005). The air permeability of the tested paper samples also correlates with print mottle in yellow and black colors.

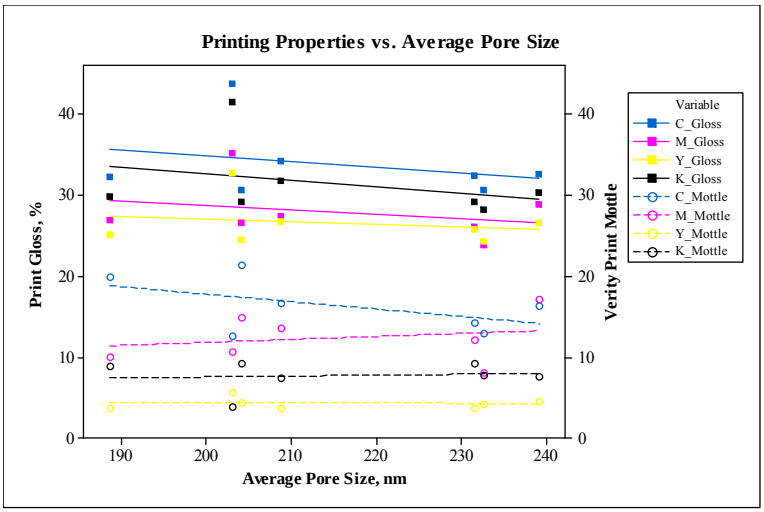

Figure 6: Relationship of average pore size vs. printing properties

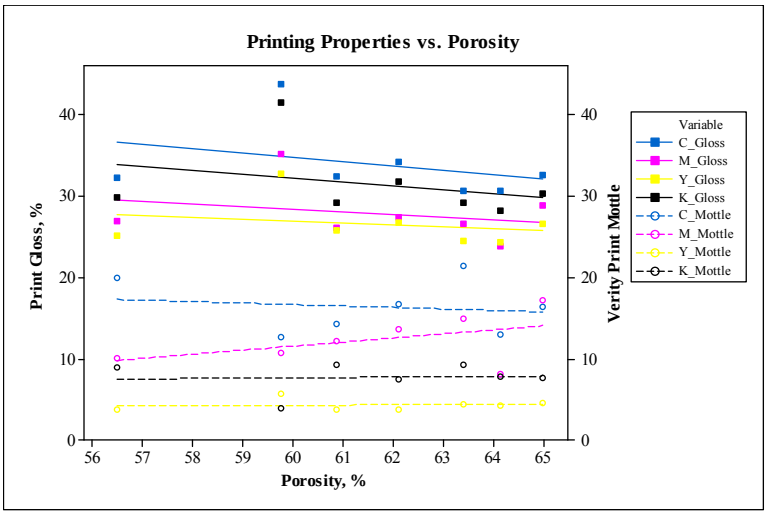

Figure 7: Relationship of porosity vs. printing properties

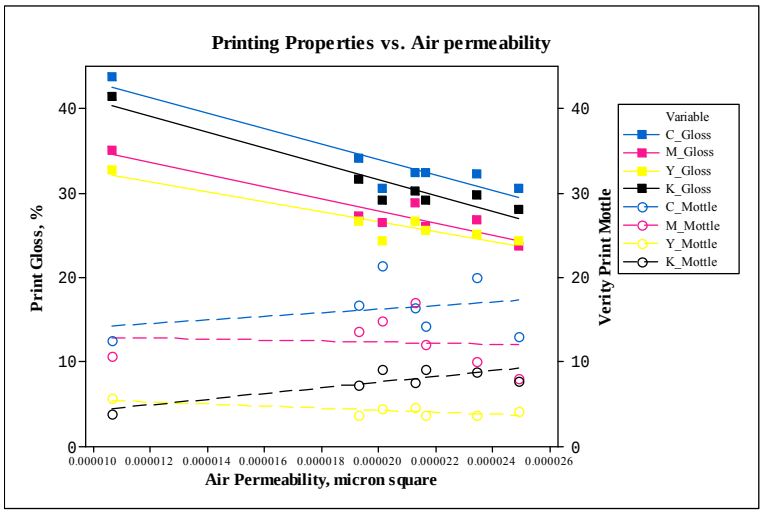

Figure 8: Relationship of air permeability vs. printing properties

Correlation Analysis for Surface Properties and Color gamut

The correlation analysis results about the relationship between the paper surface properties and color gamut are exhibited in **Table 10** and **Figure 9**. As shown in **Table 10**, the correlations between paper surface properties and color gamut were not clear (p value > α = .05). It was also shown in **Figure 9** where those points did not cluster closely around the imaginary line of best fit. These tested samples have similar surface properties and color reproduction capability.

Table 10: Pearson correlation between paper surface properties and color gamut

Paper Properties	Color Gamut Volume	
	Sig. (2-tailed)	Pearson Correlation
EMVECO Roughness	.965	-.021
Formation Index	.436	-.354
Pore Size	.836	.097
Porosity	.415	.369
Air Permeability	.614	-.234

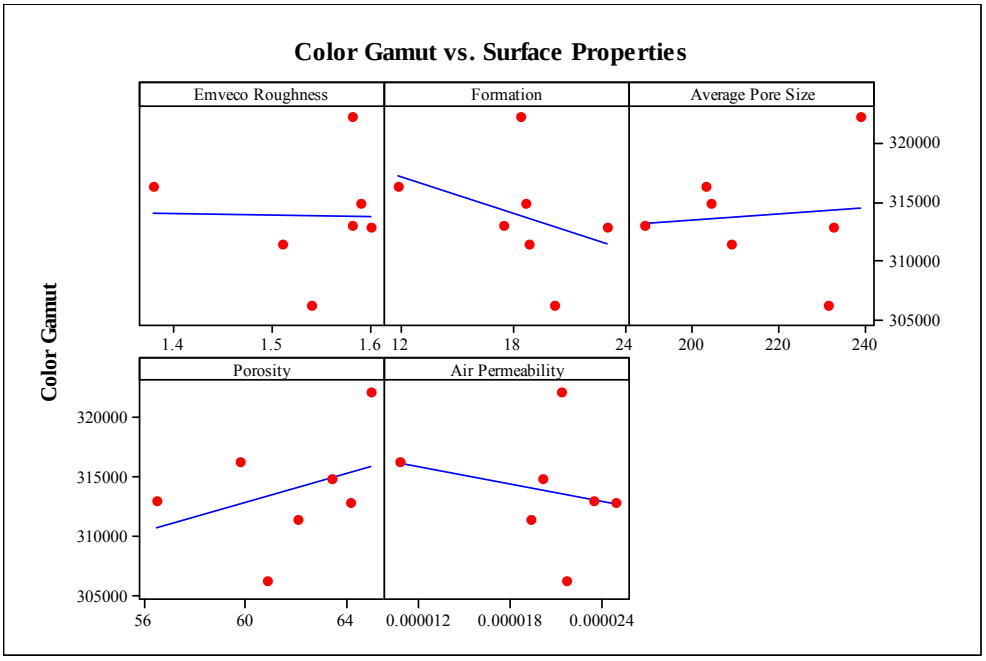

Figure 9: Relationship of surface properties vs. color gamut

CONCLUSIONS

Sample 1 produces a smoother paper surface, smaller porosity and pore size, but a less uniform paper sheet. Sample 4 yields a uniform paper sheet, but rougher paper surface and tends to have larger pore size and porosity. In terms of optical properties, sample 1 tends to have lower brightness and opacity readings. It is interesting to note that there is no significant difference in opacity among the seven types of latex polymer coating formulations.

In terms of ink-paper interaction, all paper samples have similar water absorption curves. However, the slowest penetration can be found in sample 1. Sample 1 has relatively low air permeability and smaller average pore size, which correlates with its slower penetration rate. There are obvious differences between a water ultrasound curve and a toluene ultrasound curve. For all paper samples, less toluene fluid penetrated into paper sheets. DI water penetrated into paper sheets immediately after they came into the contact with water. Sample 1 has a relatively high print gloss value and lower print mottle in cyan and black, compared to other paper samples. Sample 4 on the other hand, has lower print gloss and lower print mottle in magenta. Tested paper samples have higher print gloss values in cyan and lower print gloss readings in yellow. The print mottle in yellow of all tested paper is less obvious, compared to other colors. When it comes to color reproduction capability, the color gamuts of tested paper samples are similar to each other.

The paper surface properties such as roughness, formation, and air permeability have strong negative relationship with print gloss. However, the correlation between roughness/formation and print mottle is not clear. It was also found that there are no strong relationship between porosity/average pore size and printing properties. However, according to the data, grooved structures and convergent pore geometries seem to decrease print gloss and increase print mottle permanence. The correlations between paper surface properties and color gamut were not clear because of their similar surface properties and color reproduction capability.

To sum up, sample 1 yields a smoother paper surface, smaller porosity/pore size/air permeability and higher print gloss. But its paper sheet is less uniform and print mottle phenomena are relatively obvious in magenta and yellow colors. Further research will include possible changing coating parameters such as latex content and additives such as thickener and carboxymethyl cellulose (CMC) to improve paper sheet uniformity, print mottle, and color reproduction capability.

ACKNOWLEDGEMENTS

The author wants to thank Mike Flickinger and Michelle X. Wang for help with the coating, and WMU Printing Pilot Plant for help with the printing trial. Financial support from OMNOVA Foundation is gratefully acknowledged. Sincere appreciation is also expressed to Dr. Alexandra Pekarovicova and Dr. Paul D. Fleming from the department of Paper Engineering, Chemical Engineering, and Imaging at Western Michigan University for their helpful advice and assistance with the work.

REFERENCES

Bergh, Nils-Olaf. (1997). "Don't underestimate the power of the polymer," *Pulp & Paper Europe,* 2 (9), pp. 13-15.

Biermann, C. J. (1996). *Handbook of Pulp and Papermaking***.** San Diego: Academic Press, p. 171.

Chovancova, V., Howell, P., Fleming, P.D. ,and Rasmusson, A. (2005). "Color and Lightfastness of Different Epson Ink Jet Ink Sets", *J. Imaging Sci. Technol.,* 49 (6), pp. 652-659.

Chovancova-Lovell, V. and Fleming, P. D. (2008). "Color Gamut – New Tool in the Pressroom?", *TAPPI J*, in press.

Forbes, M., Triantafillopoulos, N. & Lallemant, T. (1998). "Modeling Latex Variables to Predict the Printing Properties of Coated Papers", *Proceedings of TAGA 50th Annual Technical Conference.* Chicago, IL. pp. 698-710.

Kentta, E., Pohler, T. & Juvonen, K. (2006). "Latex uniformity in the coating layer of paper" *Nordic Pulp and Paper Research Journal,* 21 (5), pp. 665-669.

Larsson, M. and Engstrom, G. (2004). "Interactions in coating colors based on GCC of broad and narrow particle size distribution and their effect on pore structure", *2004 TAPPI Coating and Graphic Arts Conference and Exhibit*, pp. 61-76.

Laudone, G. M., Matthews, G.. P., Gane, P. A. C. (2006). "Effect of latex volumetric concentration on void structure, particle packing and effective particle size distribution in a pigmented coating layer", *2006 TAPPI Advanced Coating Fundamentals Symposium*, pp. 251-264.

Laudone, G. M., Matthews, G.. P., Gane, P. A. C., Ridgway, C., & Schoelkopf, J. (2005). "Estimation of the effective particle sizes within a paper coating layer using a void network model" *Chemical Engineering Science*, 60 (23), pp. 6795-6802.

Lee, H. K., Joyce, M. K. & Fleming, P. D. (2005). "Influence of Pigment Particle Size and Pigment Ratio on Printability of Glossy Inkjet Paper Coatings", *Journal of Imaging Science and Technology*, 49 (1), pp. 54-61.

Levlin, J. E. & Soderhjelm, L. (2000). *Pulp and Paper Testing,* Helsinki, Finland : Fapet Oy, p. 175.

Pal, L., Joyce, M. K., & Fleming, P. D. (2006). "A Simple Method for Calculation of the Permeability Coefficient of Porous Media," *TAPPI Journal,* 6 (9), pp. 10-16.

Peel, J. D. (1999). *Paper Science and Paper manufacture,* Bellingham, WA: Angus Wilde Publications Inc, pp. 31-33.

Pohler, T., Juvonen, K. & Sneck, A. (2006). "Coating layer microstructure and location of

binder - Results from SEM analysis" *2006 TAPPI Advanced Coating Fundamentals Symposium*, pp. 79-89.

Rahman, L. (2003). "Factors Affecting the Performance of Inkjet Papers", *2003 TAPPI Spring Technical Conference & Trade Fair,* pp. 239-257.

Ratto, P. (2004). "Mechanical properties of coating layers," *Journal of Pulp and Paper Science,* 30 (12), pp. 335-340.

Rosenberger, R. (2006). The correlation of macro print mottle to surface topography as measured by an optical surface topography system, *Proceedings of the Technical Association of the Graphic Arts*, pp. 118-119.

Scott, W. E. & Abbott, J. C. (1995). *Properties of Paper: An Introduction***,** Atlanta, Georgia: TAPPI Press, p. 61.

Thompson, B. (1998). *Printing Materials: Science and Technology***,** Pira International, Leatherhead. pp. 260, 279.

Triantafillopoulos, N. & Lee, D. (1997). "Paper Coatings & Their Influence on Offset Paper and Ink Interaction", *American Ink Maker,* 75 (5): 36-38.

Vincent, E. (1996). "Binders Overview", *1996 Coating Binders Short Course***.** Atlanta, GA, TAPPI Press. pp. 1-4.

Wilson, L. A. (1997). *What the Printer Should Know about Paper,* Pittsburgh, PA: GATFPress, p. 81.

Xu, R. (2006). "The Effect of Paper Physical Properties on Print Gloss and Ink Mileage", PhD. Dissertation, Western Michigan University.

Xu, R., Fleming, P. D., Pekarovicova, A. and Bliznyuk, V. (2005). "The Effect of Ink Jet Papers Roughness on Print Gloss and Ink Film Thickness," *J. Imaging Sci. Technol.*, 49 (6), pp. 660-665.

Zang, Y. & Aspler, J. (1998). "Effect of Surface Binder Content on Print Density and Ink Receptivity of Coated Paper", *1997 Advanced Coating Fundamentals Symposium: Proceedings*, pp. 165-170.